

All-Electron Molecular Tunnel Ionization Based on the Weak-Field Asymptotic Theory in the Integral Representation

Imam S. Wahyutama,^{1,*} Denawakage D. Jayasinghe,² François Mauger,¹ Kenneth Lopata,^{2,3} and Kenneth J. Schafer¹

¹*Department of Physics and Astronomy, Louisiana State University, Baton Rouge, Louisiana 70803, USA*

²*Department of Chemistry, Louisiana State University, Baton Rouge, Louisiana 70803, USA*

³*Center for Computation and Technology, Louisiana State University, Baton Rouge, Louisiana 70808, USA*

(Dated: January 16, 2025)

Tunnel ionization (TI) underlies many important ultrafast processes, such as high-harmonic generation and strong-field ionization. Among the existing theories for TI, many-electron weak-field asymptotic theory (ME-WFAT) is by design capable of accurately treating many-electron effects in TI. An earlier version of ME-WFAT relied on an accurate representation of the asymptotic tail of the orbitals, which hindered its implementation in Gaussian-basis-set-based quantum chemistry programs. In this work, we reformulate ME-WFAT in the integral representation, which makes the quality of the asymptotic tail much less critical, hence greatly facilitating its implementation in standard quantum chemistry packages. The integral reformulation introduced here is therefore much more robust when applied to molecules with arbitrary geometry. We present several case studies, among which is the CO molecule where some earlier theories disagree with experiments. Here, we find that ME-WFAT produces the largest ionization probability when the field points from C to O, as experiments suggest. An attractive feature of ME-WFAT is that it can be used with various types of multielectron methods whether of density functional [Phys. Rev. A **106**, 052211 (2022)] or multiconfiguration types, this in turn facilitates tunnel ionization calculation in systems exhibiting a strong multireference character.

I. INTRODUCTION

In the investigation of strong-field ionization (SFI) [1–3] in many-electron systems, theoretical methods can provide an in-depth scrutiny that can both guide and illuminate experimental studies [4]. In this regard, an accurate and efficient theoretical description of tunnel ionization (TI), which is the dominant method of SFI at long wavelengths, is desirable, given the time-consuming nature of many-electron simulations in strongly driven systems. SFI, and TI in particular, is a process that is sensitive to the instantaneous field strength, making SFI a promising tool for time-resolving the study of ultrafast dynamics in molecules. Furthermore, TI is the first step in the process of high-harmonic generation [5, 6], a key mechanism underlying attosecond science.

There have been a number of efforts to develop approximate quantum mechanical theories of TI over the years, including the Ammosov-Delone-Krainov (ADK) model [7], the extension of ADK for molecular cases (MOADK) [8, 9], the Keldysh-Faisal-Reiss (KFR) method [2, 10–12], and the weak-field asymptotic theory (WFAT) [13–17]. Alternatively, in time-dependent wave function propagation methods [18–23], TI can be evaluated using absorbing masks [6], complex absorbing potentials [24–30], exterior complex scaling (ECS) [31, 32], infinite-range ECS [33, 34], or by projecting to scattering states [35–39]. Among these theoretical methods, time-dependent evolution of either wave functions or densities [40, 41] are considered to be the most accurate. These methods, however, are often very expensive since at each time-step, one

needs to construct the Hamiltonian from the two-electron integrals, which may reach more than several million for even medium-sized molecules and moderate-sized basis sets. The alternatives to time-dependent methods are much cheaper at the expense of somewhat reduced accuracy. Of particular interest here, is the WFAT, which has been shown to give satisfactory agreement with experimental orientation-dependent ionization yields [42–45].

Several flavors of WFAT have been developed, as detailed in the next section. Briefly, the one-electron (OE-)WFAT [13, 14, 16, 46] approximates the ionizing wave function with a single configuration framework while multiconfiguration effects can be treated in the many-electron (ME-)WFAT [47–49]. In WFAT, the ionization rate can be calculated using either the asymptotic portion of the wave function, called the tail representation (TR) [13, 14, 47–49], or reformulated in the so-called integral representation (IR) [46, 50, 51]. In this work, we develop a formulation of ME-WFAT that works in virtually any molecular geometry by reformulating the theory in the integral representation (IR). Specifically, by reformulating the Schrödinger equation in its integral form via the appropriate Green’s function, the resulting integral formulas allow Gaussian-type orbitals (GTO) to be used to expand the molecular orbitals (MO) without a significant loss of accuracy. This greatly reduces the requirement on the accuracy of the asymptotic tail, and is the reason for the more general applicability of the IR formulation. Thus far, the IR has only been applied in the OE-WFAT formulation [46], where angle-dependent TI from molecules as big as benzene, naphthalene [51], and phenyl rings system [52] have been successfully calculated. IR ME-WFAT therefore paves the way towards an efficient computational method of TI that is applicable

* iwahyutama@ucmerced.edu

regardless of molecular geometry and is also capable of treating the effects due to multielectron interactions. The IR ME-WFAT method presented in this work is the foundation of the DFT-based ME-WFAT in Ref. [53], where we showed that the resulting angle-dependent ionization yields are in excellent agreement with the full real-time time-dependent density functional theory calculations.

We illustrate IR-MEWFAT in a range of atoms, and small- to mid-size molecular systems. We show that the main way ME-WFAT improves angle-dependent ionization rates calculated by OE-WFAT is through the definition of the dipole moment used in the formulation and the use of Dyson orbital as the ionizing orbital. In particular, we show that angle-dependent ionization rates that are in good agreement with results from experiments or time-dependent methods in CO and N₂ can be recovered by using ME-WFAT. To demonstrate the versatility of the integral formulation for arbitrary molecular geometry, we demonstrate the computation of angle-dependent ionization rates in several polyatomic molecules, such as formic acid and CH₃F. The computer codes used for running all simulations in this work, both ME-WFAT and OE-WFAT, are currently implemented in a developer version of the NWChem quantum chemistry program [54, 55]. Another program that provides OE-WFAT capabilities is PYSTRUCTUREFACTOR [56], while the SLIMP package is developed to target more general properties of strong-field interactions with its ionization functionality implemented at the MOADK and KFR levels of theory [57, 58].

The rest of the paper is organized as follows: In section II, we detail the background in the development and comparison for the various flavors of WFAT. In section III the formulation of ME-WFAT within IR will be outlined. We will present some illustrative calculations of structure factors in Section IV, highlighting the capabilities of ME-WFAT relative to OE-WFAT. In Section IV A, we will discuss the equivalence between TR and IR ME-WFAT using some atoms as test cases. Section IV B presents cases where OE-WFAT is sufficient for TI calculation. In Section IV C and IV D, we discuss two main factors through which ME-WFAT improves OE-WFAT, these are the dipole moment and Dyson orbital. Finally, we will discuss prospective applications and improvements to IR ME-WFAT introduced in this work in Section V.

II. WFAT BACKGROUND

The earliest version of WFAT is the OE-WFAT, which is based on the single-active electron approximation [13, 14, 16]. Here, the defining problem starts from a one-electron, mean-field-type Schrödinger equation, for example, the Roothan equation in Hartree-Fock (HF) or the Kohn-Sham equation in density functional theory (DFT). Choosing the defining eigenproblem this way has two consequences: (i) Only one electron is involved in the rearrangement following the ionization that forms the final state (the orbitals other than the ionizing one are

frozen during ionization), and (ii) OE-WFAT can only be used in conjunction with single-determinant methods. This is because the orbital energy, needed in the calculation of ionization probability, is only well-defined for single-configuration wave functions. As a consequence of this, OE-WFAT can not simulate, even approximately, ionization starting from an excited initial state. To see why, recall that in a single-configuration framework, an excited state would be a configuration where an electron is moved from an occupied orbital to a virtual one. If, for example, the final state is the ground state (in which all electrons reside in the occupied orbitals), then the ionizing orbital is a virtual orbital of the initial charge state. Since virtual orbitals often have positive orbital energy, this violates the underlying assumption in WFAT that the initial energy should be negative.

WFAT has also been extended to formally include all electrons in the system, resulting in ME-WFAT [47]. In contrast to OE-WFAT, ME-WFAT takes the exact all-electron Hamiltonian as the defining eigenproblem [47]. This means the ionizing wave function is the fully antisymmetric, all-electron eigenfunction of the system. The problems with OE-WFAT mentioned in the preceding paragraph are absent in ME-WFAT. Since the wave function is no longer restricted to a single-determinant, multiconfiguration effects in TI can now be treated [48]. For example, in high-harmonic generation, a process that involves TI in its initial step, it has been found that an adequate description of correlation is required to reproduce experiments that involve resonant enhancement via ionic states [59, 60].

Instead of orbital energy, ME-WFAT uses the proper ionization potential, that is, the difference between the initial and final state eigenvalues, which is always negative if the initial state lies below the final cationic state. Therefore, ionization from an excited initial state can be handled, in addition to ionization from the ground state.

The original ME-WFAT introduced in Ref. [47] is derived under TR where the orbitals need to have an accurate representation of the asymptotic dependence at large distance (the tail of the orbital). Because of this, the original formulation of ME-WFAT poses a numerical challenge—an accurate asymptotic dependence is difficult to achieve without using grid-type basis functions. A Hartree-Fock program based on a specially designed grid exists [61] but it is only formulated for atoms and diatomic molecules. In fact, designing a grid basis that is applicable to any polyatomic molecule while still incurring a tractable amount of computations when used in conjunction with accurate multiconfiguration methods is a great challenge. That is why it has been difficult to use TR ME-WFAT for any molecules other than the two geometry groups previously mentioned. Table I summarizes the properties of the various representations of WFAT and whether one-electron or all-electron is used.

TABLE I. The comparison of the properties of WFAT types classified based on representation and the number of active electrons. In a hand-waving manner, going down the rows means broader range of molecular geometries is covered, while going to the right across columns means more accuracy because correlation becomes better described. Some related references for each type are also given.

	OE-WFAT	ME-WFAT
TR	<ul style="list-style-type: none"> - Only works with single-configuration method - Can (approximately) handle excited final state - Cannot handle excited initial state - No $2e$ integrals - Works best for atoms and diatomic molecules Ref. [13–16].	<ul style="list-style-type: none"> - Works with any number of configurations - Can handle excited initial and final states - No $2e$ integrals - Works best for atoms and diatomic molecules Ref. [47, 48, 62].
IR	<ul style="list-style-type: none"> - Only works with single-configuration method - Can (approximately) handle excited final state - Cannot handle excited initial state - Need to evaluate $2e$ integrals - No restriction on the molecular geometry Ref. [46, 50, 51].	<ul style="list-style-type: none"> - Works with any number of configurations - Can handle excited initial and final states - Need to evaluate $2e$ integrals - No restriction on the molecular geometry <i>This work.</i>

III. THEORY

A. The *first* asymptotic expansion of multielectron wave functions

We consider a many-electron molecule perturbed by an external electric field whose magnitude is such that single ionization is the dominant process. We then aim to establish a set of formulas that allow us to calculate the ionization rate as a function of field strength and the relative orientation between the molecule and the field. For one-electron WFAT, the starting equation is the Schrödinger equation for an electron subjected to an effective one-body potential, and this is often the mean-field equation that defines the orbitals. In the case of many-electron WFAT, we start from the original Schrödinger equation of an N -electron system,

$$H^{(N)}\Psi_n(Q_N) = E_n^{(N)}\Psi_n(Q_N), \quad (1)$$

where

$$H^{(N)} = -\frac{1}{2} \sum_{i=1}^N \nabla_i^2 + V^{(N)}, \quad (2)$$

$$V^{(N)}(\mathbf{R}_N) = -\sum_{i=1}^N \sum_{I=1}^{N_A} \frac{Z_I}{|\mathbf{r}_i - \mathbf{C}_I|} + \sum_{i=1}^{N-1} \sum_{j=i+1}^N \frac{1}{|\mathbf{r}_i - \mathbf{r}_j|} + \sum_{i=1}^N Fz_i, \quad (3)$$

where F is the magnitude of the external static field pointing in the positive z direction, N_A is the number of nuclei, $\mathbf{C}_1, \mathbf{C}_2, \dots, \mathbf{C}_{N_A}$ are the nuclear coordinates, and Z_1, Z_2, \dots, Z_{N_A} are their charges. The following notations for the coordinates are used throughout this

paper,

$$Q_N \equiv \{q_1, \dots, q_{N-1}, q\}, \quad (4a)$$

$$\mathbf{R}_N \equiv \{\mathbf{r}_1, \dots, \mathbf{r}_{N-1}, \mathbf{r}\}, \quad (4b)$$

$$q_i \equiv \{\mathbf{r}_i, s_i\}, \quad (4c)$$

$$q \equiv q_N. \quad (4d)$$

where $\mathbf{r}_i \equiv \{r_i, \theta_i, \varphi_i\}$ and s_i are the spatial and spin coordinates of the i -th electron. In the rest of this paper, q is synonymous to q_N (the coordinate of the last electron). It also proves to be advantageous to work in parabolic coordinate for the last electron since it allows for the separation of Schrödinger equation with a static field in the asymptotic region,

$$\xi = r + z, \quad 0 \leq \xi < \infty \quad (5a)$$

$$\eta = r - z, \quad 0 \leq \eta < \infty \quad (5b)$$

$$\varphi = \arctan \frac{y}{x}, \quad 0 \leq \varphi \leq 2\pi. \quad (5c)$$

In what follows, we chose the last electron to be the one removed due to single ionization. With the static external force pulling the electrons in the negative z direction, the ionization region (which lies in the asymptotic region) is therefore represented by $\eta \rightarrow \infty$. We will also conventionally refer to the initial molecule as the ‘neutral’ and the ionized one as the ‘cation’. However, the derivation below applies to any initial and final charge states as long as the latter has one less electron than the former.

Since we are considering single ionization, it is useful to use an *ansatz* in which the eigenfunctions of Eq. (1) are expanded in terms of a basis that factorizes into an antisymmetrized product between an $(N-1)$ -electron function and a one-electron function,

$$\Psi_n(Q_N) = \sum_{n'} \frac{N!}{(N-1)!} \hat{\mathcal{A}} \left(\tilde{\Psi}_{n'}(Q_{N-1}) t_{n'n}(q) \right), \quad (6)$$

where \hat{A} is the antisymmetrization operator. The function $t_{n'n}(q)$, in which all information about the ionized electron will be encoded, is expressed as a linear combination of *parabolic channel functions* $\Phi_\nu^{n'n}(\xi, \varphi)$,

$$t_{n'n}(\eta, \xi, \varphi, s) = \frac{1}{\sqrt{\eta}} \sum_\nu F_{\nu\sigma}^{n'n}(\eta) \Phi_\nu^{n'n}(\xi, \varphi) \chi_\sigma(s), \quad (7)$$

and is the unknown that we will partially solve in the following analysis (it will be a partial solution because we are only interested in the asymptotic region relevant for ionization). The sum in Eq. (7) runs over all parabolic quantum number pairs $\nu \equiv (n_\xi, m)$, $n_\xi = 0, 1, \dots$, $m = 0, \pm 1, \dots$ [13, 14], and $\sigma \in \{\alpha, \beta\}$ is the z -projection of the spin angular momentum, hence $\alpha = 1/2$ and $\beta = -1/2$. σ implicitly depends on n' due to the requirement that, together with the spin projection of $\tilde{\Psi}_{n'}$, it must produce the spin projection of Ψ_n . Eq. (7) is the many-electron generalization of Eq. (11) in Ref. [15]. The parabolic channel function is the solution of the following eigen equation

$$\mathcal{B}^{n'n} \Phi_\nu^{n'n}(\xi, \varphi) = \beta_\nu^{n'n} \Phi_\nu^{n'n}(\xi, \varphi), \quad (8)$$

where

$$\mathcal{B}^{n'n} = \frac{\partial}{\partial \xi} \left(\xi \frac{\partial}{\partial \xi} \right) + \frac{1}{4\xi} \frac{\partial^2}{\partial \varphi^2} + \frac{\text{IP}_{n'n} \xi}{2} - \frac{F\xi^2}{4} + Z_c,$$

and thus may be written as

$$\Phi_\nu^{n'n}(\xi, \varphi) = \phi_{n_\xi|m}^{n'n}(\xi) \frac{e^{im\varphi}}{\sqrt{2\pi}}. \quad (9)$$

Several remarks on the form of Eq. (6) are in order. This equation is in a general form because, even though it has been expressed in the most suitable way for single ionization, it still allows for a straightforward generalization to higher order ionization. If simultaneous double ionization is desired, for instance, one can reexpress Eq. (6) so that the basis is in the form of $\hat{A}(\tilde{\Psi}_{n'}(Q_{N-2})t_{n'n}(q, q'))$. The expansion in Eq. (6) also includes the localized and delocalized contributions to $\Psi_n(Q_N)$. An example of localized contributions would be the contributions from the bound states of the unperturbed neutral molecule. In this case, the densities of both $\tilde{\Psi}_{n'}$ and $t_{n'n}$ are localized near the nuclei. The case of ionization focuses on the delocalized terms on the RHS of Eq. (6).

Evaluating Eq. (6) in the asymptotic region ($\eta \rightarrow \infty$) will quench any terms on the RHS for which $t_{n'n}(q)$ is localized, leaving only terms for which $t_{n'n}(q)$ is delocalized, while $\tilde{\Psi}_{n'}(Q_{N-1})$ can be either localized or delocalized. Imposing the single ionization approximation will suppress the latter, hence we are left with terms for which $t_{n'n}(q)$ is delocalized and $\tilde{\Psi}_{n'}(Q_{N-1})$ is localized. Since $\tilde{\Psi}_{n'}(Q_{N-1})$ is localized, without loss of generality, we can use the eigenstates of the $(N-1)$ -electron Hamiltonian in its place, i.e. $\tilde{\Psi}_{n'} \rightarrow \Psi_{n'}^+$, where $\Psi_{n'}^+$ is an eigenstate of $H^{(N-1)}$. Because $\Psi_{n'}^+$ is local, in the region $\eta \rightarrow \infty$ the

exchange interaction between the ionized electron and the bound ones dies away, and the antisymmetric product in Eq. (6) reduces to an ordinary product,

$$\hat{A}(\Psi_{n'}^+(Q_{N-1})t_{n'n}(q))|_{\eta \rightarrow \infty} \approx \frac{(N-1)!}{N!} \Psi_{n'}^+(Q_{N-1})\tau_{n'n}(q), \quad (10)$$

where we have defined $\tau_{n'n}(q) \equiv t_{n'n}(q)|_{\eta \rightarrow \infty}$. Therefore, in the asymptotic region Eq. (6) has the form of

$$\Psi_n(Q_N)|_{\eta \rightarrow \infty} = \sum_{n'} \Psi_{n'}^+(Q_{N-1})\tau_{n'n}(q). \quad (11)$$

Note that on the RHS, only $\tau_{n'n}(q)$ is evaluated asymptotically, whereas the final eigenstate $\Psi_{n'}^+$ stays bound.

In order to solve for $\tau_{n'n}(q)$, the first step is to substitute the asymptotic wave function in Eq. (11) into Eq. (1) in the asymptotic region,

$$H^{(N)}|_{\eta \rightarrow \infty} \Psi_n(Q_N)|_{\eta \rightarrow \infty} = E_n^{(N)} \Psi_n(Q_N)|_{\eta \rightarrow \infty}. \quad (12)$$

where

$$H^{(N)}|_{\eta \rightarrow \infty} = H^{(N-1)} - \frac{\nabla^2}{2} - \frac{Z_c}{r} + O(r^{-2}) + Fz, \quad (13)$$

$$Z_c = \sum_{I=1}^{N_A} Z_I - N + 1,$$

We note that the terms represented by $O(r^{-2})$ in Eq. (13) above contains the dipole term of the asymptotic expansion of $V^{(N)}(\mathbf{R}_N)$. This dipole term will be omitted from this point onward because we are interested in the lowest order approximation of ME-WFAT. This term becomes important when one considers the first order correction [62]. By using Eq. (11) in Eq. (12) and then projecting to a particular final eigenstate, one obtains

$$\left(-\frac{\nabla^2}{2} - 2\frac{Z_c}{\eta + \xi} - \frac{1}{2}F(\eta - \xi) - \text{IP}_{n'n} \right) \tau_{n'n}(q) = 0 \quad (14)$$

where $\text{IP}_{n'n} = E_n^{(N)} - E_{n'}^{(N-1)}$ is the ionization potential, and we have applied the change of coordinate to the parabolic coordinate system.

Using Eq. (7), (8), and (9), Eq. (14) can be simplified to an equation satisfied by $F_{\nu\sigma}^{n'n}(\eta)|_{\eta \rightarrow \infty}$,

$$\left(\frac{\partial^2}{\partial \eta^2} + \frac{F\eta}{4} + \frac{\text{IP}_{n'n}}{2} \right) F_{\nu\sigma}^{n'n}(\eta)|_{\eta \rightarrow \infty} = 0 \quad (15)$$

where the $O(\eta^i)$ terms with $i = -1, -2$ have been dropped since they are negligible in the asymptotic region. Eq. (15) can be transformed to the Airy differential equation and thus its solution can be expressed in terms of the asymptotic form of the Airy function,

$$F_{\nu\sigma}^{n'n}(\eta)|_{\eta \rightarrow \infty} = \frac{\sqrt{2} f_{\nu\sigma}^{n'n}}{(F\eta)^{1/4}} \exp \left(\frac{i\sqrt{F}}{3} \eta^{3/2} + \frac{i\text{IP}_{n'n}}{\sqrt{F}} \sqrt{\eta} \right). \quad (16)$$

Eq. (11) along with Eq. (7) and (16) constitute the asymptotic expansion of the perturbed neutral wave function $\Psi_n(Q_N)$ interacting with an external static field pointing in the positive z direction in terms of some asymptotic basis functions weighted by $f_{\nu\sigma}^{n'n}$. Since in WFAT this coefficient is interpreted as the ionization probability, the goal of any WFAT derivation is then to construct an expression for the expansion coefficients $f_{\nu\sigma}^{n'n}$ in terms of the field strength and orientation, as well as the unperturbed properties of the system such as the unperturbed ionization energy, dipole moment, and wave functions. The next section is devoted to obtaining such an expression for $f_{\nu\sigma}^{n'n}$ within the integral formulation of ME-WFAT.

B. The second asymptotic expansion of multielectron wave functions

In Section III A, we derived an asymptotic expansion of the initial wave function interacting with a static electric field pointing in the positive z direction (also shown in Eq. (30) below). In this section, we will first obtain another form of the asymptotic expansion for $\Psi_n(Q_N)|_{\eta \rightarrow \infty}$ different from that derived in Section III A. But since these two expansions are equivalent, comparing them should yield the sought expression for $f_{\nu\sigma}^{n'n}$.

As the first step, note that Eq. (1) can be rewritten as

$$\left(H_{\text{ref}} - E_n^{(N)}\right) \Psi_n(Q_N) = -V_c(\mathbf{R}_N) \Psi_n(Q_N) \quad (17)$$

where

$$H_{\text{ref}} = H^{(N-1)} - \frac{\nabla^2}{2} - \frac{Z_c}{r} + Fz + O(r^{-2}), \quad (18)$$

$$V_c(\mathbf{R}_N) = V_{1e}(\mathbf{r}) + V_{2e}(\mathbf{R}_N) + O(r^{-2}), \quad (19)$$

$$V_{2e}(\mathbf{R}_N) = \sum_{i=1}^{N-1} \frac{1}{|\mathbf{r} - \mathbf{r}_i|}, \quad (20)$$

$$V_{1e}(\mathbf{r}) = -\sum_{I=1}^{N_A} \frac{Z_I}{|\mathbf{r} - \mathbf{C}_I|} + \frac{Z_c}{r}. \quad (21)$$

We note that the $O(r^{-2})$ terms in Eq. (18) and (19) are identical, and are incorporated to account for the dipole term of $V^{(N)}(\mathbf{R}_N)$. For the same argument regarding the $O(r^{-2})$ term in Eq. (13), this higher multipole term will be omitted in this work. One might notice that the various potential terms in Eq. (19)-(21) are not entirely origin-independent. This is because of the multipole expansion of the core potential, which gives rise to the origin-dependent terms, such as the Z_c/r and the dipole potential term contained in $O(r^{-2})$. As has been shown in Ref. [14, 50], for wave functions having the exact asymptotic behavior, the structure factor and hence the ionization rate are origin-independent (see also Section IIID).

In the integral form, Eq. (17) (or equivalently, Eq. (1)) takes the form

$$\Psi_n(Q_N) = -\int dQ'_N G_n(Q'_N; Q_N) V_c(\mathbf{R}'_N) \Psi_n(Q'_N) \quad (22)$$

where the Green's function $G_n(Q'_N; Q_N)$ is the solution of the following inhomogeneous equation

$$\left(H_{\text{ref}} - E_n^{(N)}\right) G_n(Q'_N; Q_N) = \prod_{i=1}^N \delta(\mathbf{r}'_i - \mathbf{r}_i) \delta_{s'_i s_i}. \quad (23)$$

We note that the integral solution of the type of Eq. (22) is the corner stone of the integral representation of OE-WFAT and ME-WFAT introduced in the present work. Because this integral integrates over the entire $4N$ dimensions, one is not presented with the difficulty found in the TR associated with the incomplete integration leaving the η coordinate unintegrated. This leads to the TR ionization rates becoming sensitive to the accuracy of the asymptotic tail (that occupies the unintegrated dimension) of the wave function.

The next step is to solve for $G_n(Q'_N; Q_N)$ for which we will use the following spectrally resolved *ansatz*,

$$G_n(Q'_N; Q_N) = -\frac{2}{\sqrt{\eta'\eta}} \sum_{n'\nu} \Psi_{n'}^+(Q_{N-1}) (\Psi_{n'}^+(Q'_{N-1}))^* \mathcal{G}_{\nu}^{n'n}(\eta, \eta') \Phi_{\nu}^{n'n}(\xi, \varphi) \Phi_{\nu}^{n'n}(\xi', \varphi') \chi_{\sigma}(s) \chi_{\sigma}^{\dagger}(s') \quad (24)$$

where $\bar{\nu} \equiv (n_{\xi}, -m)$ and $\mathcal{G}_{\nu}^{n'n}(\eta, \eta')$ is a one-dimensional Green's function that we are going to solve for. Substituting Eq. (24) into Eq. (23), and following similar steps to Ref. [46], one arrives at the following differential equation

$$\left(\frac{\partial^2}{\partial \eta^2} + \frac{1-m^2}{4\eta^2} + \frac{\text{IP}_{n'n}}{2} + \frac{F\eta}{4} + \frac{\beta_{\nu}^{n'n}}{\eta}\right) \mathcal{G}_{\nu}^{n'n}(\eta, \eta') = \delta(\eta - \eta'). \quad (25)$$

As a side note, the differential operator in the LHS of Eq. (25) is identical to the one that gives rise to Eq. (15) before omitting the $O(\eta^i)$ terms, with $i = -1, -2$.

In order so that $\mathcal{G}_{\nu}^{n'n}(\eta, \eta')$ is uniquely defined through Eq. (25), we must impose boundary conditions on this equation. A physically meaningful choice is that $\mathcal{G}_{\nu}^{n'n}(\eta, \eta')|_{\eta \rightarrow 0} \in [0, \infty)$ and $\mathcal{G}_{\nu}^{n'n}(\eta, \eta')|_{\eta \rightarrow \infty} = 0$. We also denote the two linearly independent solutions to the homogeneous equation that arises from Eq. (25) when $\eta \neq \eta'$ as $R_{\nu}^{n'n}(\eta)$ and $O_{\nu}^{n'n}(\eta)$. We then arbitrarily assign $R_{\nu}^{n'n}(\eta)$ to the solution that is regular at $\eta = 0$, hence $0 \leq R_{\nu}^{n'n}(0) < \infty$, and $O_{\nu}^{n'n}(\eta)$ to the one that vanishes as $\eta \rightarrow \infty$, hence $\lim_{\eta \rightarrow \infty} O_{\nu}^{n'n}(\eta) = 0$. There are a number of known methods for solving the Green's function of a second order differential equation [63]. Using these methods, it can be shown that the solution of

Eq. (25), satisfying the aforementioned boundary conditions, is

$$\mathcal{G}_\nu^{n'n}(\eta, \eta') = \begin{cases} O_\nu^{n'n}(\eta') R_\nu^{n'n}(\eta) / \mathcal{W}_\nu^{n'n} & , 0 \leq \eta < \eta' \\ R_\nu^{n'n}(\eta') O_\nu^{n'n}(\eta) / \mathcal{W}_\nu^{n'n} & , \eta > \eta' \end{cases} \quad (26)$$

with the Wronskian $\mathcal{W}_\nu^{n'n}$ defined to be

$$\begin{aligned} \mathcal{W}_\nu^{n'n} &= R_\nu^{n'n}(\eta) \frac{dO_\nu^{n'n}(\eta)}{d\eta} - O_\nu^{n'n}(\eta) \frac{dR_\nu^{n'n}(\eta)}{d\eta} \\ &= \text{constant} \end{aligned} \quad (27)$$

The Wronskian being constant follows from the absence of the first order derivative term in the differential Eq. (25) [63]. From Eq. (26), we obtain

$$\mathcal{G}_\nu^{n'n}(\eta, \eta') \Big|_{\eta \rightarrow \infty} = \frac{R_\nu^{n'n}(\eta')}{\mathcal{W}_\nu^{n'n}} O_\nu^{n'n}(\eta) \Big|_{\eta \rightarrow \infty}. \quad (28)$$

To obtain $O_\nu^{n'n}(\eta) \Big|_{\eta \rightarrow \infty}$, we note that it is a solution of Eq. (25) when the RHS is set to zero and when $\eta \rightarrow \infty$. But these conditions make this equation identical to Eq.

(15), implying that $O_\nu^{n'n}(\eta) \Big|_{\eta \rightarrow \infty}$ must have the same form as Eq. (16) with the only difference being in the constant prefactor (given that Eq. (15) is homogeneous). This means, in Eq. (16), we can arbitrarily make a replacement $f_{\nu\sigma}^{n'n} \rightarrow O_\nu^{n'n}$ in the RHS, and identify the LHS as $O_\nu^{n'n}(\eta) \Big|_{\eta \rightarrow \infty}$. Applying this to Eq. (28) results in

$$\begin{aligned} \mathcal{G}_\nu^{n'n}(\eta, \eta') \Big|_{\eta \rightarrow \infty} &= \frac{O_\nu^{n'n}}{\mathcal{W}_\nu^{n'n}} R_\nu^{n'n}(\eta') \frac{\sqrt{2}}{(F\eta)^{1/4}} \\ &\times \exp\left(i \frac{\sqrt{F}}{3} \eta^{3/2} + i \frac{\text{IP}_{n'n}}{\sqrt{F}} \eta^{1/2}\right). \end{aligned} \quad (29)$$

By substituting Eq. (29) into (24), and then Eq. (24) into (22), we have essentially arrived at a new asymptotic expansion for $\Psi_n(Q_N)$ with the unknown being the coefficient $O_\nu^{n'n}$. To facilitate a clearer picture of where we are within the derivation process so far, we will explicitly write down these two different-looking but equivalent asymptotic expansions. The first one, which is formed with the help of Eq. (11), (7), and (16), reads

$$\Psi_n(Q_N) \Big|_{\eta \rightarrow \infty} = \frac{1}{\sqrt{\eta}} \sum_{n'} \frac{\sqrt{2}}{(F\eta)^{1/4}} \exp\left(i \frac{\sqrt{F}}{3} \eta^{3/2} + i \frac{\text{IP}_{n'n}}{\sqrt{F}} \eta^{1/2}\right) \Psi_{n'}^+(Q_{N-1}) \sum_{\nu\sigma} \Phi_\nu^{n'n}(\xi, \varphi) \chi_\sigma(s) f_{\nu\sigma}^{n'n}, \quad (30)$$

while the second one, which is formed through the use of Eq. (22), (24), and (29), reads

$$\begin{aligned} \Psi_n(Q_N) \Big|_{\eta \rightarrow \infty} &= \frac{1}{\sqrt{\eta}} \sum_{n'} \frac{\sqrt{2}}{(F\eta)^{1/4}} \exp\left(i \frac{\sqrt{F}}{3} \eta^{3/2} + i \frac{\text{IP}_{n'n}}{\sqrt{F}} \eta^{1/2}\right) \Psi_{n'}^+(Q_{N-1}) \sum_{\nu\sigma} \Phi_\nu^{n'n}(\xi, \varphi) \chi_\sigma(s) \\ &\times \left\{ \frac{2O_\nu^{n'n}}{\mathcal{W}_\nu^{n'n}} \int dQ'_N \frac{R_\nu^{n'n}(\eta')}{\sqrt{\eta'}} \Phi_\nu^{n'n}(\xi', \varphi') \chi_\sigma^\dagger(s') (\Psi_{n'}^+(Q'_{N-1}))^* V_c(\mathbf{R}'_N) \Psi_n(Q'_N) \right\}. \end{aligned} \quad (31)$$

Eq. (30) and (31) have been arranged such that all common quantities are written first. Comparing these two equations, it is clear that the coefficient $f_{\nu\sigma}^{n'n}$ is equal to the terms inside the curly brackets in Eq. (31), which may also be understood to be the many-electron generalization of Eq. (54) in Ref. [46].

C. The leading order weak-field approximation

Despite having obtained a closed form expression for $f_{\nu\sigma}^{n'n}$, the various terms inside the curly brackets in Eq. (31), such as the initial and final wave functions, among others, are still not yet straightforwardly calculable because these terms are associated with a Hamiltonian that has an external DC field term. In addition, the corre-

sponding Schrödinger equation for general multielectron systems cannot be easily solved due to the need of the continuum eigensubspace of the unperturbed Hamiltonian. This is the point where the weak-field approximation is invoked.

In this approximation, the field is assumed to be weak enough compared to the binding force of the nuclei, therefore the quantities that depend on the field strength can be expanded in powers of the field, the same way any

perturbation-type expansion is performed, namely

$$\Psi_n = \Psi_n^{(0)} + F\Psi_n^{(1)} + O(F^2) \quad (32a)$$

$$\Psi_n^+ = \Psi_n^{+(0)} + F\Psi_n^{+(1)} + O(F^2) \quad (32b)$$

$$E_n^{(N)} = E_n^{(N)(0)} - F\mu_{nz}^{(N)} + O(F^2) \quad (32c)$$

$$R_\nu^{n'n} = R_\nu^{n'n(0)} + FR_\nu^{n'n(1)} + O(F^2) \quad (32d)$$

$$\Phi_\nu^{n'n} = \Phi_\nu^{n'n(0)} + F\Phi_\nu^{n'n(1)} + O(F^2) \quad (32e)$$

$$\beta_\nu^{n'n} = \beta_\nu^{n'n(0)} + F\beta_\nu^{n'n(1)} + O(F^2) \quad (32f)$$

and a similar definition as $E_n^{(N)}$ applies to $E_{n'}^{(N-1)}$. The Wronskian, within the weak-field approximation, can be shown to be

$$\mathcal{W}_\nu^{n'n} = -\varkappa = -\sqrt{2|\text{IP}_{n'n}^{(0)}|} \quad (33)$$

with $\text{IP}_{n'n}^{(0)} = E_n^{(N)(0)} - E_{n'}^{(N-1)(0)}$, the field-free ionization potential [46]. $\mu_{nz}^{(N)}$ is the z -component of $\boldsymbol{\mu}_n^{(N)}$, the total electronic dipole moment corresponding to $|\Psi_n^{(0)}\rangle$ in the lab-frame. Apart from $\mu_{nz}^{(N)}$, we will also need $\boldsymbol{\mu}_{n'z}^{(N-1)}$, the total electronic dipole moment of $|\Psi_{n'}^{+(0)}\rangle$ in the lab-frame. These dipole vectors are given by

$$\boldsymbol{\mu}_n^{(N)} = -\left\langle \Psi_n^{(0)} \left| \sum_{i=1}^N \hat{\mathbf{r}}_i \right| \Psi_n^{(0)} \right\rangle, \quad (34)$$

$$\boldsymbol{\mu}_{n'}^{(N-1)} = -\left\langle \Psi_{n'}^{+(0)} \left| \sum_{i=1}^{N-1} \hat{\mathbf{r}}_i \right| \Psi_{n'}^{+(0)} \right\rangle. \quad (35)$$

The $O_\nu^{n'n}$ coefficient has been solved by employing the *connection formula* in a previous work on WFAT [15]. The derivation in the case of IR ME-WFAT is completely parallel to that in the aforementioned reference, with the only difference being the definition of orbital energy and dipole moments involved in the derivation. We therefore refer the readers to these references for the details of obtaining $O_\nu^{n'n}$. Here, we simply invoke the final result for the leading order term, which reads

$$O_\nu^{n'n(0)} = \sqrt{\frac{\varkappa}{2}} \left(\frac{4\varkappa^3}{F} \right)^{\beta_\nu^{n'n(0)}/\varkappa} \times \exp \left(i\frac{\pi}{4} + i\frac{\pi\beta_\nu^{n'n(0)}}{\varkappa} - \mu_z^{n'n}\varkappa - \frac{\varkappa^3}{3F} \right), \quad (36)$$

where $\beta_\nu^{n'n(0)} = Z_c - \varkappa \left(n_\xi + \frac{|m|+1}{2} \right)$ and $\mu_z^{n'n}$ is the lab-frame z -component of the vector difference $\boldsymbol{\mu}_n^{(N)} - \boldsymbol{\mu}_{n'}^{(N-1)}$. This appearance of dipole moment difference in ME-WFAT within the integral representation is consistent with the tail representation [47], and can also be found in other TI theories that incorporate Stark shift correction [64–66]. We note that the factor

$(4\varkappa^3/F)^{\beta_\nu^{n'n(0)}/\varkappa}$ in Eq. (36) is different from that in Eq. (50) in Ref. [46] in which the power of \varkappa is 2, instead of 3. As can be checked by rederiving Eq. (59) in the aforementioned paper, the correct power of \varkappa is 3 (as appears in Eq. (36) above).

Now that we have everything we need to construct the leading order approximation to the coefficient $f_{\nu\sigma}^{n'n}$, we can substitute Eq. (33), Eq. (36), and the zeroth order terms in Eq. (32) for the corresponding terms inside the curly brackets in Eq. (31). This yields,

$$f_{\nu\sigma}^{n'n(0)} = \sqrt{\frac{\varkappa}{2}} \left(\frac{4\varkappa^2}{F} \right)^{\beta_\nu^{n'n(0)}/\varkappa} g_{\nu\sigma}^{n'n}(\beta, \gamma) \times \exp \left(i\frac{\pi}{4} + i\frac{\pi\beta_\nu^{n'n(0)}}{\varkappa} - \mu_z^{n'n}\varkappa - \frac{\varkappa^3}{3F} \right) \quad (37)$$

where the *asymptotic coefficient* $g_{\nu\sigma}^{n'n}$ is defined as

$$g_{\nu\sigma}^{n'n}(\beta, \gamma) = -2\varkappa\beta_\nu^{n'n(0)}/\varkappa-1 \int dQ_N \frac{R_\nu^{n'n(0)}(\eta)}{\sqrt{\eta}} \times \Phi_\nu^{n'n(0)}(\xi, \varphi) \chi_\sigma^\dagger(s) \left(\Psi_{n'}^{+(0)}(Q_{N-1}) \right)^* \times V_c(\mathbf{R}_N) \Psi_n^{(0)}(Q_N). \quad (38)$$

Of particular interest is the structure factor, defined by

$$G_{\nu\sigma}^{n'n}(\beta, \gamma) = e^{-\varkappa\mu_z^{n'n}} g_{\nu\sigma}^{n'n}(\beta, \gamma), \quad (39)$$

which is a field-independent quantity and is largely a molecule-specific parameter that determines the shape of the ionization probability as a function of orientation angle.

We note that in Eq. (38), the orientation dependence is encoded in the orientation of $|\Psi_n^{(0)}\rangle$, $|\Psi_{n'}^{+(0)}\rangle$, and \hat{V}_C relative to $\Omega_\nu^{n'n}(\mathbf{r}) = R_\nu^{n'n(0)}(\eta) \Phi_\nu^{n'n(0)}(\xi, \varphi)/\sqrt{\eta}$, which is fixed in space since it is contingent to the lab-frame z -axis. This means, for every orientation angle of interest, one needs to rotate the $3N$ and $3(N-1)$ dimensional wave functions and potential. A more efficient but equivalent method is to fix the wave functions and potential, but rotate $\Omega_\nu^{n'n}(\mathbf{r})$ instead. To perform this three-dimensional rotation, we follow a partial wave expansion method employed in [51]

$$g_{\nu\sigma}^{n'n}(\beta, \gamma) = \sum_{l=|m|}^{\infty} \sum_{m'=-l}^l I_{\nu l m' \sigma}^{n'n} d_{m m'}^l(\beta) e^{-im'\gamma} \quad (40)$$

where

$$I_{\nu l m' \sigma}^{n'n} = \int dQ_N \tilde{R}_{\nu l}^{n'n}(r) Y_{l m'}^*(\theta, \varphi) \chi_\sigma^\dagger(s) \times \left(\Psi_{n'}^{+(0)}(Q_{N-1}) \right)^* V_c(\mathbf{R}_N) \Psi_n^{(0)}(Q_N), \quad (41)$$

$$\tilde{R}_{\nu l}^{n'n}(r) = \omega_{\nu l}^{n'n}(\varkappa r)^l e^{-\varkappa r} M(l+1-Z/\varkappa, 2l+2, 2\varkappa r),$$

$d_{mm'}^l(\beta)$ is the Wigner function [67], $Y_{lm}(\theta, \varphi)$ is the spherical harmonics, $M(a, b, x)$ is the confluent hypergeometric function [68], and

$$\begin{aligned} \omega_{\nu l}^{n' n} &= (-1)^{l+(|m|-m)/2+1} 2^{l+3/2} \varkappa^{Z/\varkappa-(|m|+1)/2-n_\xi} \\ &\times \sqrt{(2l+1)(l+m)!(l-m)! (|m|+n_\xi)! n_\xi!} \\ &\times \frac{l!}{(2l+1)!} \sum_{k=0}^{\min(n_\xi, l-|m|)} \frac{1}{k!(l-k)! (|m|+k)!} \\ &\times \frac{\Gamma(l+1-Z/\varkappa+n_\xi-k)}{(l-|m|-k)!(n_\xi-k)!}. \end{aligned}$$

is a normalization coefficient. To compute the integral in Eq. (41), the integration over Q_{N-1} and s_N is performed analytically, while the integration over \mathbf{r}_N is done with the help of a combination of Becke fuzzy cells [69] and quadrature grids [51].

As has been mentioned earlier, the WFAT ionization probability is origin-independent provided that the asymptotic behavior of the wave functions is exact. For all simulations presented in this work, we use Gaussian-type orbitals (GTO), which are excellent for representing local properties but are poor for simulating asymptotic behavior. For this reason, the origin-independence in GTO-based WFAT results is only approximate. We can, however, minimize this effect by following the previous works (*e.g.* see Ref. [50]) where the origin is chosen so that

$$\mathbf{D}_{n'}^{(N-1)} = \sum_{I=1}^{N_A} Z_I \mathbf{C}_I - \boldsymbol{\mu}_{n'}^{(N-1)} = 0, \quad (42)$$

here, $\mathbf{D}_{n'}^{(N-1)}$ is the total dipole of the final charge state. All simulations presented here are performed in the frame where $\mathbf{D}_{n'}^{(N-1)} = 0$.

Concluding this section, we briefly discuss the mathematical structure of the expressions for the asymptotic coefficient in IR ME-WFAT and TR ME-WFAT. First, in the case of OE-WFAT, both the IR (see Eq. (20) in Ref. [46]) and the TR (see Eq. (59) in Ref. [46]) formulas explicitly show a dependence on the ionizing orbital, which is one of the initial charge state orbitals. In ME-WFAT, the ionizing orbital is the Dyson orbital. The dependence of the asymptotic coefficient on the orbital is explicit in TR ME-WFAT (see Eq. (43) below) while in IR ME-WFAT, it is partially explicit (see Eq. (41)). It is only partially explicit because as will be shown in Section III F, the 1-electron term, $V_{1e}(\mathbf{r})$, will lead to the appearance of the Dyson orbital, but the 2-electron term, $V_{2e}(\mathbf{R}_N)$, will not. Despite this property, we will show in Section III F that the present formulation of ME-WFAT in the IR is consistent with that in the TR.

D. The asymptotic cancellation problem

The hallmark of TR WFAT (whether one- or many-electron) is the exact cancellation in the asymptotic re-

gion between a certain exponential pre-factor and another function that depends on the ionizing orbital. For this reason, the asymptotic part of the ionizing orbital needs to be as close as possible to being the inverse of the exponential pre-factor. For instance, in the TR ME-WFAT, the structure factor is given by

$$\begin{aligned} g_{\nu\sigma}^{n'n} &= \left[\eta^{1/2-\beta_\nu^{n'(0)}/\varkappa} e^{\varkappa\eta/2} \int_0^\infty \int_0^{2\pi} d\xi d\varphi \phi_\nu^{n'n(0)}(\xi) \right. \\ &\times \left. \frac{e^{im\varphi}}{\sqrt{2\pi}} \psi_D^\sigma(\mathbf{r}) \right] \Bigg|_{\eta \rightarrow \infty} \end{aligned} \quad (43)$$

[47] where

$$\psi_D^\sigma(\mathbf{r}) = \int dQ_{N-1} ds \left(\Psi_{n'}^{+(0)}(Q_{N-1}) \chi_\sigma(s) \right)^* \Psi_n^{(0)}(Q_N)$$

is the Dyson orbital. In the above equation, the integral over s is to be understood as a vector scalar product. The exact asymptotic behavior of the Dyson orbital is that it decays as $\exp -\varkappa\eta/2$ [49], hence asymptotically cancelling the exponential function in Eq. (43). For approximate many-electron initial and/or final wave functions, however, the exponent $\tilde{\varkappa}$ appearing in the asymptotic tail of the corresponding Dyson orbital is not necessarily equal to \varkappa . This may cause $g_{\nu\sigma}^{n'n}$ either to vanish ($\tilde{\varkappa} > \varkappa$) or to diverge ($\tilde{\varkappa} < \varkappa$).

The above cancellation problem has been discussed in Ref. [49]. There, the many-electron wave functions are calculated at the Hartree-Fock level, in which the Dyson orbital is just a linear combination of the occupied orbitals. The asymptotic part of such a linear combination is therefore given by that of the least bound orbital, which has the largest coefficient, *i.e.* $\tilde{\varkappa} = \sqrt{2|\epsilon|} \neq \varkappa$ where ϵ is the orbital energy of the least bound occupied orbital. To ensure that a finite value of the asymptotic coefficient can be extracted, Tolstikhina *et al.* [49] imposes $\tilde{\varkappa} = \sqrt{2|\epsilon|} = \varkappa$. The situation becomes more complicated when a configuration interaction (CI) wave function is used since in this case, orbitals having lower binding energy appear in the Dyson orbital linear combination. These orbitals decay slower than HF HOMO, which causes an imperfect cancellation in the asymptotic region.

In IR ME-WFAT, the equation used to calculate the asymptotic coefficient (Eq. (38) or (40)) involves integration over the entire $4N$ space-spin coordinates, in contrast to the TR ME-WFAT version in Eq. (43) that leaves η unintegrated. The fact that these integrals in IR ME-WFAT are over all space means that the asymptotic part of the Dyson orbital is no longer crucial in determining the convergence of the integration, which further implies that Gaussian standard basis functions can be used to span the orbital space making up the multielectron wave functions. It is also for the same reason that, when the one-electron approximation is sufficient, the IR OE-WFAT [46, 50, 51] is more practical than the TR version for polyatomic molecular tunnel ionization problems.

Lastly, although it is still a topic for future studies, the use of CI wave functions will be much more manageable in IR ME-WFAT compared to TR ME-WFAT [49].

E. Ionization rate

The difference between TR and IR lies in the method to calculate the asymptotic coefficient, while the fundamental assumption on how the ionization probability is extracted remains unchanged. Thus, the ionization rate formula is the same as in TR [47], namely

$$\Gamma = \sum_{n'\sigma\nu} N |f_{\nu\sigma}^{n'n(0)}|^2 + O(\Gamma^2). \quad (44)$$

Eq. (44) above gives the ionization rate of an electron originating from the initial state $|\Psi_n\rangle$ to a number of final states $|\Psi_{n'}^+\rangle$ having one less electron. The presence of the multiplier N in Eq. (44) accounts for the indistinguishability of the ionized electrons.

F. Application to single-determinant wave functions

It is important to note that no assumptions are imposed on the unperturbed wave functions $|\Psi_n\rangle$ and $|\Psi_{n'}^+\rangle$ appearing in Eq. (41) other than being an eigenstate of the respective all-electron Hamiltonian—both can take any structure, whether single (Hartree-Fock or DFT [53]) or multideterminant. Since determinants are the building blocks of many correlated wave function methods, in this section, IR ME-WFAT will be applied to the calculation of the asymptotic coefficient when both the initial and final wave functions are a single (Slater) determinant.

In this case, we have

$$\Psi(Q_N) = \frac{1}{\sqrt{N!}} \det \left(\psi_{i_1}^\alpha \cdots \psi_{i_{N_\alpha}}^\alpha \psi_{i_1}^\beta \cdots \psi_{i_{N_\beta}}^\beta \right), \quad (45a)$$

$$\Psi^+(Q_{N-1}) = \frac{1}{\sqrt{(N-1)!}} \det \left(v_{i_1}^\alpha \cdots v_{i_{N'_\alpha}}^\alpha v_{i_1}^\beta \cdots v_{i_{N'_\beta}}^\beta \right) \quad (45b)$$

where $N = N_\alpha + N_\beta$, $N - 1 = N'_\alpha + N'_\beta$, and we have omitted the eigenstate index from the two wave functions since the HF method produces only one meaningful determinant. Each spin orbital is a product state between the spatial and spin functions, *e.g.* $v_i^\beta \equiv v_i^\beta(\mathbf{r})\chi_\beta(s)$. Since the ionized electron is assumed to have a definite z -component of spin, we have $N'_\sigma = N_\sigma - 1$ and $N'_{p(\sigma)} = N_{p(\sigma)}$. Here, the spin channel where an electron has been removed (that is, the *ionized spin channel*) is denoted by σ , while $p(\sigma)$ is the *unionized spin channel* and has values such that $p(\alpha) = \beta$ and $p(\beta) = \alpha$.

We note that with the help of Eq. (19), $I_{\nu l m' \sigma}^{n' n}$ can be decomposed into two- and one-electron terms,

$$I_{\nu l m' \sigma}^{n' n} = \left\langle \Psi^+; \Omega_{l m' \sigma}^\nu \chi_\sigma \left| \hat{V}_{1e} \right| \Psi \right\rangle + \left\langle \Psi^+; \Omega_{l m' \sigma}^\nu \chi_\sigma \left| \hat{V}_{2e} \right| \Psi \right\rangle \quad (46)$$

Then, the integrals over the first $N - 1$ electron coordinates as well as s_N are carried out analytically while the one over \mathbf{r}_N is done numerically using numerical quadrature. The former involves extensive determinant algebra, and thus we will only cite the results of Appendix A here. By first defining $\Omega_{l m' \sigma}^\nu(\mathbf{r}) = \hat{R}_{\nu l}(r) Y_{l m'}(\theta, \varphi)$, the two-electron component reads

$$\begin{aligned} \left\langle \Psi^+; \Omega_{l m' \sigma}^\nu \chi_\sigma \left| \hat{V}_{2e} \right| \Psi \right\rangle = & \frac{\delta_{M'_s + m_\sigma, M_s}}{\sqrt{N}} (-1)^{N + \delta_{\sigma\beta} N_\alpha} \\ & \times \left\{ \mathcal{R} \sum_{k'=1}^{N_\sigma-1} \sum_{j=2}^{N_\sigma} \sum_{k=1}^{j-1} (-1)^{j+k+k'} \mathcal{Q}(k, j, k') \right. \\ & \times \left(\left\langle \Omega_{l m' \sigma}^\nu \left| \hat{V}_{k'k}^{\sigma} \right| \psi_j^\sigma \right\rangle - \left\langle \Omega_{l m' \sigma}^\nu \left| \hat{V}_{k'j}^{\sigma} \right| \psi_k^\sigma \right\rangle \right) + \\ & \left. \left\langle \Omega_{l m' \sigma}^\nu \left| \hat{\mathcal{V}}^\sigma \right| \tilde{\psi}^\sigma \right\rangle \right\} \quad (47) \end{aligned}$$

and for the 1-electron term, it reads

$$\left\langle \Psi^+; \Omega_{l m' \sigma}^\nu \chi_\sigma \left| \hat{V}_{1e} \right| \Psi \right\rangle = \delta_{M'_s + m_\sigma, M_s} \left\langle \Omega_{l m' \sigma}^\nu \left| \hat{V}_{1e} \right| \psi_D^\sigma \right\rangle. \quad (48)$$

where $\mathcal{Q}(k, j, k')$ is the determinant of the overlap matrix in the *ionized spin channel* between the initial wave function after removing $\{\psi_k^\sigma, \psi_j^\sigma\}$ and the final wave function after removing $\{v_{k'}^\sigma\}$, \mathcal{R} is the determinant of the overlap matrix in the *un-ionized spin channel* between the initial and final eigenstates, $\hat{V}_{k'k}^{\sigma}$ is the electrostatic repulsion operator due to the $(v_{k'}^\sigma(\mathbf{r}))^* \psi_k^\sigma(\mathbf{r})$ charge density, and $\hat{\mathcal{V}}^\sigma$ is the repulsion operator of the electrons in the spin- $p(\sigma)$ channel. For more details, see Appendix A. In Eq. (47), k' runs over the occupied spatial orbitals in the spin- σ channel of the final state whereas j and k run over the occupied spatial orbitals in the spin- σ channel of the initial state.

A brief discussion of the various terms appearing in the RHS of Eq. (47) is in order. First, the first and second terms inside the curly bracket represent the electron-electron interaction (repulsion and exchange) felt by the ionized electron in its own spin channel (spin- σ channel). The third term may be viewed as the repulsion due to the electrons in the spin- $p(\sigma)$ channel felt by the ionized electron. There is no cross-channel exchange term, that is, the exchange between the ionized electron and those in the spin- $p(\sigma)$ channel, which is a well-known property associated with the use of single-determinant wave functions.

We are now at the point where we can show that IR ME-WFAT is equivalent to IR OE-WFAT in a certain

limit. This is when all of the occupied spin orbitals of the final HF wave function are a subset of the occupied spin orbitals of the initial HF wave function, in other words when the final cationic determinant is unrelaxed. If we assume that the only spin orbital that is unoccupied in the final HF wave function is $|\psi_{i'}^\sigma\rangle$, then the determinant coefficients defined in Eq. (A4) reduce to

$$\mathcal{P}(i) = \delta_{ii'} \quad (49a)$$

$$\mathcal{R} = 1 \quad (49b)$$

$$\mathcal{Q}(k, i, k') = (1 - \delta_{ik})(\delta_{ii'}\delta_{k'\bar{k}} + \delta_{ki'}\delta_{k'\bar{i}}) \quad (49c)$$

$$\mathcal{S}(k, k') = \delta_{k'k} \quad (49d)$$

where $\bar{i} = i$ if $i < i'$ and $\bar{i} = i - 1$ otherwise. \bar{k} has the same definition as \bar{i} with all occurrences of i replaced by k , except for i' . Then, by Koopman's theorem, the ionization potential is equal to the orbital energy of $|\psi_{i'}^\sigma\rangle$. The electronic dipole moment difference is then also equal to the dipole moment of $|\psi_{i'}^\sigma\rangle$. As is shown in Appendix B, by putting Eq. (49) into Eq. (48) and (47), one recovers the integral terms valid for IR OE-WFAT (*e.g.* see Eq. (31), (21), (32)-(34) in Ref. [50]). Concluding this section, we have obtained the integral formulas necessary to calculate ME-WFAT ionization rate in the integral representation when the initial and final wave functions are both single Slater determinants.

IV. RESULTS AND DISCUSSION

In TR ME-WFAT, it is clear that the Dyson orbital is central in determining the angular dependence of the structure factor (see Eq. (43)). On the other hand, in IR ME-WFAT, the significance of this orbital may not be directly apparent (*cf.* Eq. (38)). Reflecting the central role played by the Dyson orbital in ME-WFAT, we use it as one of the components of analyses presented in this section. In this regard, we introduce the ratio

$$r = \left| \frac{\mathcal{P}(i_{2\text{nd max}})}{\mathcal{P}(i_{\text{max}})} \right|, \quad (50)$$

where i_{max} and $i_{2\text{nd max}}$ are the indices of the largest and second-largest expansion coefficients of the Dyson orbital, respectively (see Eq. (A10) and (A6)). This ratio may be interpreted as the degree of similarity of the Dyson orbital to one of the occupied MO of the initial state. For general multiconfiguration wave functions, two factors influence r : (1) relaxation effect, and (2) multireference effect. In the present work where all states are single-determinant, only (1) applies. The other component of our analysis is the dipole moment because the dipole moments used in OE-WFAT and in ME-WFAT may have different directions and as will be shown below, this affects the relative magnitude of the ionization rates between the parallel and antiparallel directions.

Some of the systems considered below are doubly degenerate, these are O₂, OCS, and CH₃F. In the exact

treatment, their degeneracies will be broken by the ionizing field, however, in the leading order approximation of WFAT assumed in this work, only field-free wave functions and orbitals are used with any degeneracies still intact. It is only when one goes beyond the leading order approximation, should the field-induced modification on the orbitals be taken into account, possibly removing any degeneracies [15, 62]. The neutral and cation wave functions employed in all of the results are obtained from a HF calculation, thus representing a ground-state-to-ground-state ionization channel, and the formulas derived in Section III F have been used.

A. Atoms

In this section, we will first validate IR ME-WFAT by comparing atomic asymptotic coefficients with those obtained by TR ME-WFAT in Ref. [49]. The asymptotic coefficients of He, Li, Be, Na, and Mg calculated at the HF level for ionization starting from the neutral and ending up in the cation are presented in Table II. In the table, p is a constant pre-factor arising from the fact that in HF, one can ionize an electron with two (one) possible spin orientations when the neutral has no (one) unpaired electrons. g_{00} in Table II is obtained by multiplying the asymptotic coefficient calculated by Eq. (38) (or Eq. (40)) with \sqrt{p} , while $R = \mathcal{P}(i_{\text{max}})\mathcal{R}$ and \varkappa is given by Eq. (33). R may be considered as a measure of the influence of relaxation on the cation wave function, with the maximum value of unity representing the situation where the final state is unrelaxed. g_{00} constitutes the result of IR ME-WFAT as formulated in the present work. We compare g_{00} with g_{ref} , which is the TR ME-WFAT asymptotic coefficient extracted from Ref. [49]. The agreement is generally promising with the largest difference being about 6% found for Mg among the atoms simulated.

The values of g_{ref} in Table II were calculated by using ϵ , the orbital energy of the least bound occupied orbital instead of the actual ionization potential in Eq. (33) ($\varkappa \Rightarrow \tilde{\varkappa} = \sqrt{2|\epsilon|}$) [49]. One may therefore speculate that if we do the same substitution wherever \varkappa appears in the integral formulation derived in this work, then the agreement may get better. The results of this substitution of ionization potential with the least bound orbital energy are shown in the 6th and 7th columns of Table II. As one can see, for He, Be, and Mg, the agreement between \tilde{g}_{00} and the reference value improves as one goes down the table with the relative errors of 10.7%, 3.3%, and 1.8%, respectively. On the other hand the agreement between g_{00} with the reference value gets worse along the same direction with the relative errors of 1.9%, 4.9%, and 6.0%. This shows that the substitution $\varkappa \Rightarrow \tilde{\varkappa}$ does not guarantee improvement of the agreement between IR ME-WFAT and TR ME-WFAT [49], which further implies that the results presented in this section (as well as those that follow) are not totally identical to what

TABLE II. The asymptotic coefficients of He, Li, Be, Na, and Mg calculated by IR ME-WFAT (g_{00} and \tilde{g}_{00}) and TR ME-WFAT (g_{ref}). aug-pc-3 basis were employed for these simulations except for Li where cc-pvtz is used. This is because HF calculation of Li using aug-pc-3 gives wrong valence orbital ordering.

Atom	p	R	\varkappa	g_{00} ^a	$\tilde{\varkappa}$	\tilde{g}_{00} ^b	g_{ref} ^c
He	2	0.984	1.312 78	2.885	1.354 96	2.626	2.942
Li	1	1.000	0.626 61	0.474	0.626 66	0.474	0.474
Be	2	0.984	0.768 84	1.324	0.786 46	1.437	1.392
Na	1	1.000	0.603 23	0.416	0.603 58	0.416	0.415
Mg	2	0.985	0.696 75	1.022	0.711 32	1.068	1.087

^a This work, using the proper value of \varkappa given by Eq. (33).

^b This work, replacing the field-free ionization potential in Eq. (33) with ϵ , the orbital energy of the least bound occupied orbital.

^c The value calculated in Ref. [49] using TR ME-WFAT.

they would be if they had been obtained through the tail representation formulation. We identify the source of this imperfect equivalence as being due to the level of approximation to the all-electron wave functions involved in the calculation (Hartree-Fock level). In TR ME-WFAT, the information on the cation wave function enters solely through the Dyson orbital (see Eq. (43)), whereas in IR ME-WFAT, apart from the Dyson orbital, it also enters through the matrix element of the one-body Coulomb potential (the $\hat{V}_{k'j}^{\sigma}$ terms in Eq. (47)). To reconcile this difference in the mathematical structure of the two representations, it is conceivable that the level of approximations to the all-electron wave functions should play a role in bringing the equivalence closer or farther away. We would like to emphasize, however, that this inequivalence will disappear as one uses more and more accurate all-electron wave functions for the neutral and cation.

In Table II, Li and Na present an exception in which their g_{00} and g_{ref} are essentially identical, although HF wave functions are used. The reason is that, as can be seen from their values of R , which is unity, the HF procedure for the cation of these atoms produces orbitals that are almost identical to those making up the neutral HF wave function, that is, the cation is almost unrelaxed. In that case, both TR and IR ME-WFAT reduces to OE-WFAT.

B. O₂

For single configuration wave functions, OE-WFAT is a special case of ME-WFAT where the cation configuration is formed out of a subset of $N - 1$ orbitals of the occupied orbitals of the neutral. It should then be expected that in molecules where this condition is nearly satisfied, the structure factors calculated by OE-WFAT

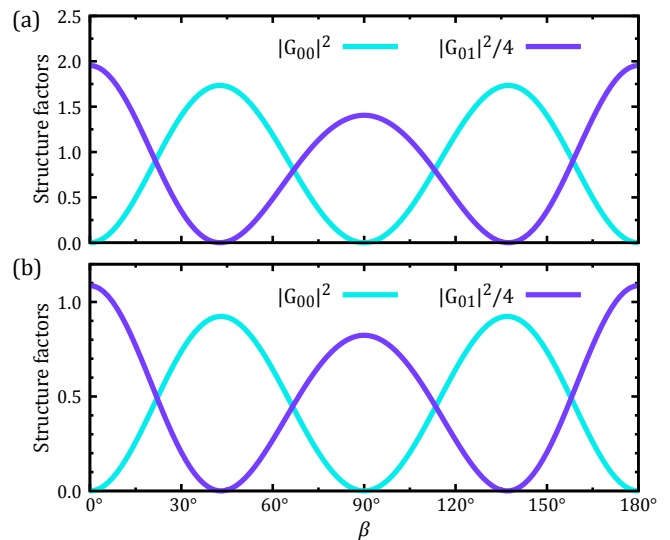


FIG. 1. Structure factors of O₂ simulated using (a) OE-WFAT and (b) ME-WFAT. In (a), HOMO from Hartree-Fock calculation of O₂ is used. The structure factors in (a) and (b) are a slice at a constant γ , which is the direction of the lobe of HOMO and Dyson orbital density, respectively. When $\beta = 0^\circ$, the field is parallel with the molecular axis.

and ME-WFAT should be similar. In this section, we show that O₂ falls within this group of molecules.

Fig. 1(a) shows the structure factor for the parabolic channel $(n, m) = (0, 0)$ and $(n, m) = (0, 1)$ of O₂ calculated using OE-WFAT and a bond length of 1.158 Å. The orbital used for this calculation is the HOMO, which is doubly degenerate and has a π_g symmetry. The symmetry is reflected in the shape of the structure factor $|G_{00}|^2$ exhibiting two peaks at $\beta = 42^\circ$ and $\beta = 138^\circ$, and a mirror symmetry around $\beta = 90^\circ$. The ionization yield of O₂ interacting with an oscillating electric field of low intensity simulated using TDCI in Ref. [29] has a very similar double-peak structure located at 45° and 135° . The shape as well as the position of these peaks also agrees with the experiments on O₂ reported in Ref. [70]. The ME-WFAT results shown in Fig. 1(b) are very similar to the one-electron counterpart in panel (a) for both parabolic channels shown, with the only difference being the magnitude. In fact, the r ratio for O₂ obtained by HF is zero, with the largest coefficient belonging to HOMO, making the O₂ Dyson orbital essentially the HOMO itself. The basis set, the ratio r , the largest and second-largest contributors to the Dyson orbital, and the ionization potentials used in ME-WFAT or OE-WFAT for O₂ as well as other molecules studied here are summarized in Table III.

Angle-dependent ionization yields of O₂ have also been studied in the context of field-induced multielectron polarization effects (MEP) in Ref. [71]. It was found that MEP has negligible effects on the angle-dependent yield of O₂. Although MEP is not considered in this work—remember that only field-free orbitals enter the formu-

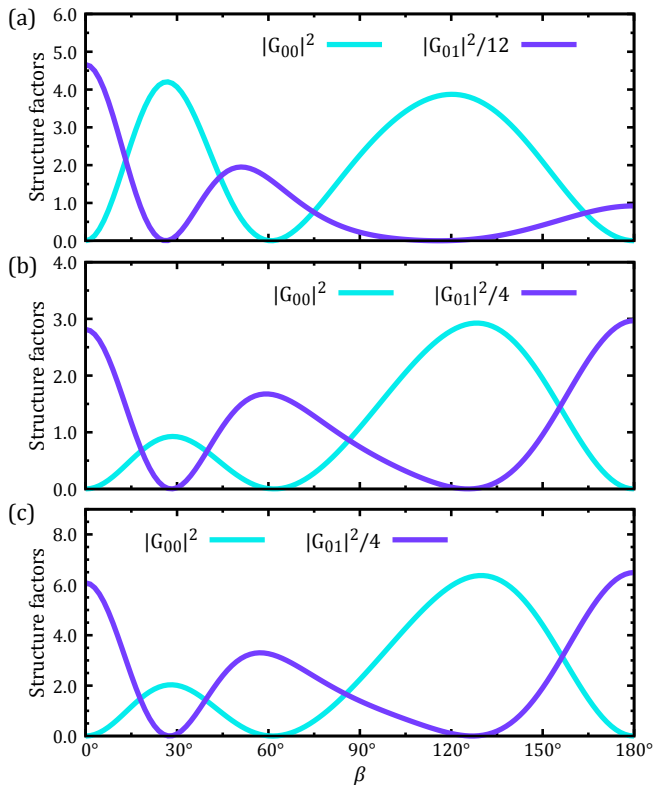


FIG. 2. Structure factors of OCS simulated using (a) OE-WFAT and (b) ME-WFAT. In (a), HOMO from Hartree-Fock calculation of OCS is used. (c) The structure factors calculated with OE-WFAT but where the definitions for the dipole moment and origin use those from ME-WFAT. The structure factors in (a), (b), and (c) are a slice at a constant γ , which is the direction of the lobe of the ionizing orbital (the Dyson orbital in ME-WFAT or the HOMO in OE-WFAT) density.

lation, this observation agrees with ours in that multi-electron effects are negligible in the ionization from the ground state of O_2 to that of its cation. To formally incorporate MEP in WFAT framework, one must include the 1st order correction of ME-WFAT, which, however, lies outside the scope of the present work, but will be studied in a future publication.

C. OCS and CO

As mentioned in Section I, there are two main reasons why the shape of the angle-dependent ionization probability obtained by ME-WFAT may differ substantially from OE-WFAT: (i) the dipole moment and (ii) the dissimilarity between the HOMO and the Dyson orbital. The present and the next sections are devoted to illustrating the effect of each of these factors on the angular variation of the structure factor.

We first look at OCS, whose HOMO has a π symmetry and is doubly degenerate. OCS is one of the most frequently studied molecules for its strong-field ioniza-

tion properties [38, 39, 53, 72, 73]. In our simulations, we choose the O-C and C-S bond lengths to be 1.123 Å and 1.564 Å, respectively. The double-peak structure of $|G_{00}|^2$ obtained by OE-WFAT seen in Fig. 2(a) is a manifestation of the π symmetry of the HOMO. The structure factors obtained by ME-WFAT (Fig. 2(b)) still retain the same general features as OE-WFAT (Fig. 2(a)) for both parabolic channels simulated here but this time the magnitude of the peak of the G_{00} channel around $\beta \sim 125^\circ$ is three times larger than the other peak. Here, we will show that this difference is largely due to the different treatment of the dipole moment in the two methods. We run a OE-WFAT simulation but this time, the origin and dipole moment are chosen according to ME-WFAT prescription. This means that the origin is such that $\mathbf{D}^{(N-1)} = 0$ and the dipole moment is given in the explanation immediately following Eq. (35). The rest, such as the orbital and integral formulas, are the same as those used to obtain Fig. 2(a). The structure factors resulting from these modifications to OE-WFAT are shown in Fig. 2(c). We see that in the case of OCS, mixing the OE-WFAT prescription for orbital and integral formula with the ME-WFAT prescription for the origin and dipole moment closely recovers the shape of the structure factors obtained by ME-WFAT.

We note that alignment-dependent rates, rather than orientation-dependent ones, of OCS seem to be more commonly calculated or measured [38, 72–74]. In these alignment-dependent curves, the maximum occurs at $\beta = 90^\circ$. Approximately emulating an alignment-dependent rate from our orientation-dependent rate $|G_{00}|^2$ in Fig. 2(b), however, produces a pair of peaks at $\beta = 38^\circ$ and $\beta = 142^\circ$ instead. The absence of a maximum at $\beta = 90^\circ$ in our result is due to insufficient suppression of the secondary peak at $\beta = 28^\circ$ in the orientation-dependent curve of Fig. 2(b) and the global maximum in the same figure occurring at a slightly too large of an angle β . Despite this discrepancy in the alignment-dependent curve, our orientation-dependent curves of OCS calculated through IR-MEWFAT (Fig. 2(b)) and DFT-based IR-MEWFAT [53] agree with RT-TDDFT result (see Ref. [53]). In our opinion, a comparison of orientation-dependent rates, rather than alignment-dependent ones, should offer a higher confidence level since weak structures in the latter tend to get washed out due to the incoherent sum of rates from opposite orientations.

Next, we turn to CO whose HOMO has a σ symmetry. We choose the C-O bond length to be 1.102 Å. The OE-WFAT and ME-WFAT structure factors are shown in Fig. 3(a) and 3(b), respectively, and we see a contrasting behavior in the location of the global maximum. IR OE-WFAT predicts that the ionization should be maximum at $\beta = 180^\circ$ (as does the TR OE-WFAT in Ref. [14, 17]), that is, when the field points from O to C, while ME-WFAT predicts the opposite. It is interesting to note that a recent calculation on CO has also been done addressing the effect of the field-induced MEP [75] on ionization yields. One of the findings in Ref. [75] is

TABLE III. The basis set, the r ratio (Eq. (50)), the largest and 2nd largest neutral’s MO, and ionization potential (IP) of the molecules studied in this work. The IP’s are in hartree, and the values to the left and right of the slash sign is the IP for ME-WFAT and OE-WFAT, respectively.

Species	Basis set	r	i_{\max}	$i_{2\text{nd max}}$	IP ⁽⁰⁾
O ₂	aug-cc-pvqz	0.0	HOMO	–	–0.470329 / –0.537404
OCS	aug-cc-pvqz	0.050	HOMO	HOMO-2	–0.369409 / –0.416889
CO	aug-cc-pvqz	0.114	HOMO	HOMO-2	–0.478264 / –0.551712
N ₂	aug-cc-pvqz	0.030	HOMO-1	HOMO-3	–0.578156 / –0.628166
HCOOH	pc-3	0.198	HOMO	HOMO-5	–0.368459 / –0.474097
CH ₃ F	pc-3	0.588	HOMO	HOMO-2	–0.455863 / –0.529495

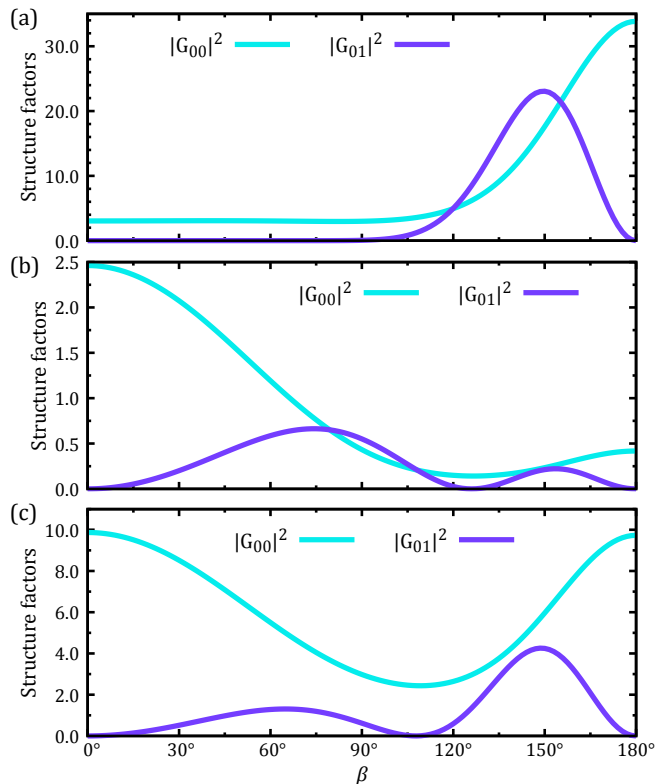


FIG. 3. Structure factors of CO simulated using (a) OE-WFAT and (b) ME-WFAT. In (a), the HOMO from Hartree-Fock calculation of CO is used. (c) The structure factors calculated with OE-WFAT but where the definitions for the dipole moment and origin use those from ME-WFAT. When $\beta = 0^\circ$, the field points from C to O.

that without MEP, the angle-resolved ion yield from CO looks very similar to $|G_{00}|^2$ in Fig. 3(a), whereas with MEP, the ion yield resembles closely $|G_{01}|^2$ of Fig. 3(b). Experiments [76] as well as time-dependent Hartree-Fock [77] calculations also produce angle-resolved ionization of CO in which the ionization is most favorable when the field points from C to O, and their shape is very similar to the yield with MEP in Ref. [75] and $|G_{00}|^2$ in Fig. 3(b). What is interesting here is that the IR ME-WFAT introduced in this work does not capture MEP effects.

Repeating the procedure we used for OCS, which mixes the origin and dipole moment of ME-WFAT with the orbital and integral formula of OE-WFAT, we obtain the structure factors in Fig. 3(c). Unlike the case of OCS for which this procedure results in structure factors that nearly reproduce the ME-WFAT results, the structure factors of both parabolic channels for CO seem to only approximate the corresponding ME-WFAT structure factors in Fig. 3(b). We attribute this disagreement to the non-negligible contribution of the next largest element of $\mathcal{P}(i)$ after $\mathcal{P}(\text{HOMO})$, which is $\mathcal{P}(\text{HOMO-2})$ with $r = 0.114$ (see Table III). For comparison, for OCS this ratio is 0.050. This observation, along with the one in the previous paragraph, are hints that, in addition to the inclusion of field-induced MEP effects (which requires the first order correction of WFAT), the correct treatment of the permanent dipole moment, as is already captured by ME-WFAT in the leading order approximation, and an accurate representation of the ionizing orbital (in ME-WFAT, the Dyson orbital) are the missing features in the methods that fail to reproduce the experimental data.

We would like to emphasize that the marked change of the structure factors when the origin and dipole moment are changed, *e.g.* from Fig. 3(a) to Fig. 3(c) or from Fig. 2(a) to Fig. 2(c), should not be viewed as the failure of ME-WFAT to be origin-independent (which is a necessary property of physical quantities such as ionization rate). When one changes the origin, the dipole moment $\mu_z^{n'n}$, the monopole term Z_c/r (see the discussion following Eq. (21)), and the center of $R_\nu^{(0)}(\eta)\Phi_\nu^{(0)}(\xi, \varphi)$ must also be transformed accordingly. In the preceding analysis however, instead of using the properly shifted dipole moment, we use the dipole moment value calculated by ME-WFAT. In fact, we have checked that the OE-WFAT structure factors resulting from shifting the origin and also properly shifting the dipole moment according to the origin shift give results very close to the original OE-WFAT results—Fig. 3(a) for CO and Fig. 2(a) for OCS. The analysis employed in the current section that mixes ME-WFAT’s origin and dipole moment with OE-WFAT’s orbital and integral formula may therefore be viewed as an improper specification of dipole moment, and an *ad hoc* procedure at best.

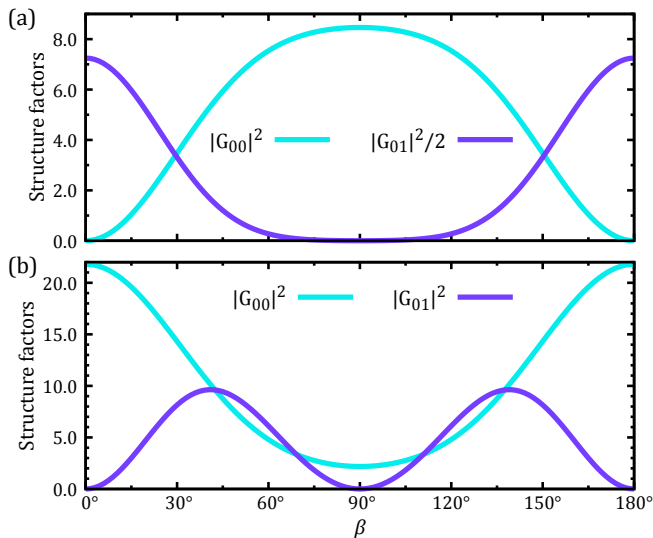


FIG. 4. Structure factors of N_2 simulated using (a) OE-WFAT and (b) ME-WFAT. In (a), HOMO from Hartree-Fock calculation of N_2 is used. The structure factors in (a) are a slice at a constant γ , which is the direction of the lobe of the HOMO density. When $\beta = 0^\circ$, the field is parallel with the molecular axis.

D. N_2 , HCOOH, and CH_3F

In the previous section, we demonstrated that for some molecules, ME-WFAT structure factors differ from the OE-WFAT counterpart mostly by the value of the dipole moment used in the exponential factor of Eq. (37). In these cases, ME-WFAT structure factors may be recovered by deliberately using the ME-WFAT dipole moment and origin in the OE-WFAT formulation. We will now show that ME-WFAT and OE-WFAT calculations can differ much less trivially when the Dyson orbital connecting the neutral and cation ground states notably differ from the neutral HOMO.

It is well-known that the occupied MO of N_2 calculated by HF have an incorrect ordering—experiments suggested that the first ionization from N_2 should produce a Σ cation state, while Koopman’s theorem says that the first ionization should leave the cation in a Π state [70, 78, 79]. See Ref. [70] for an experimental orientation-dependent ionization yield of N_2 . In the context of OE-WFAT where the ionizing orbital must be chosen manually, the HF simulation for N_2 can lead to the wrong angle-dependent ionization yield because the π character of the false HOMO will obviously dominate since it has the lowest binding energy. Using a N–N bond length of 1.066 Å, we run OE-WFAT calculation N_2 and obtain Fig. 4(a) where we see that OE-WFAT $|G_{00}|^2$ calculated using the HOMO of N_2 exhibits a π_u symmetry. Fig. 4(b) shows the results of ME-WFAT, where $|G_{00}|^2$ is seen to have the correct σ symmetry. The structure factors shown in Fig. 4(b) also look very similar to those obtained by OE-WFAT using HOMO-1 of N_2 [14].

The reason of the success of ME-WFAT in this case is that the Dyson orbital, being a linear combination of the occupied MO of the neutral, has the largest component (largest $|\mathcal{P}(i)|$) that corresponds to HOMO-1 (see Table III). In a sense, the overlap integral between the neutral and cation states defining the Dyson orbital automatically selects HOMO-1 as the orbital that is closest to the actual ionizing orbital. This result also illustrates how a properly relaxed cation wave function can facilitate the construction of an accurate ionizing orbital.

Next, we examine HCOOH (formic acid), a planar molecule (see Fig. 5(e)). The atomic coordinates in angstrom when $(\beta, \gamma) = (0^\circ, 0^\circ)$ are C: (0, 0, 0.415), O: (0, -1.011, -0.437), O: (0, 1.139, 0.110), H: (0, -0.372, 1.444), and H: (0, -0.658, -1.322). According to Ref. [80], formic acid is a good candidate to study the difference between using the Dyson orbital and the HOMO to calculate the ionization rate due to the notable contribution of occupied orbitals other than the HOMO in the linear combination of Eq. (A6). $|G_{00}|^2$ resulting from an ionization from the HOMO calculated with OE-WFAT is shown in Fig. 5(a). It features a single lobe centered around $(\beta, \gamma) = (67^\circ, 90^\circ)$. The ME-WFAT version of this structure factor is shown in Fig. 5(b), where we see that the single lobe seen in Fig. 5(a) persists. The most notable difference with OE-WFAT is the appearance of a second, weaker lobe centered around $(\beta, \gamma) = (128^\circ, 270^\circ)$ and the ‘leakage’ of the main lobe toward $\beta = 0^\circ$. These features, which are absent in the OE-WFAT structure factor, indicate that there are some occupied orbitals of the neutral that interfere with the dominating HOMO in forming the ionizing orbital. Fig. 5(f) and 5(g) compare the shapes of HOMO and Dyson orbital, respectively, with Fig. 5(h) presenting the individual contribution of some of the most important occupied orbitals of the neutral in terms of their coefficient, $\mathcal{P}(i)$, in the linear combination of Eq. (A6).

We see that the contribution of HOMO-5 is not so small compared to the largest contribution coming from HOMO. The contribution from HOMO-5 to the Dyson orbital is most likely also responsible for the sharp difference in the magnitude of $|G_{00}|^2$ calculated by OE-WFAT (Fig. 5(a)) and ME-WFAT (Fig. 5(b)). This can be seen from OE-WFAT structure factor from HOMO-5 shown in Fig. 5(d), where we see that it has a maximum at about the same orientation as the structure factor in Fig. 5(a) [81]. This may suggest that the regions of HOMO and HOMO-5 that are responsible for their respective orientation of maximum ionization rate interfere in a way that drastically reduces the maximum ionization probability from the Dyson orbital. There is another MO that produces maximum ionization at about the same angle as HOMO and HOMO-5, namely HOMO-4, whose OE-WFAT structure factor is shown in Fig. 5(c). However, its corresponding $\mathcal{P}(i)$ is significantly smaller than that of HOMO-5.

As the last example, we examine CH_3F , a molecule having an equilibrium geometry that possesses a C_{3v}

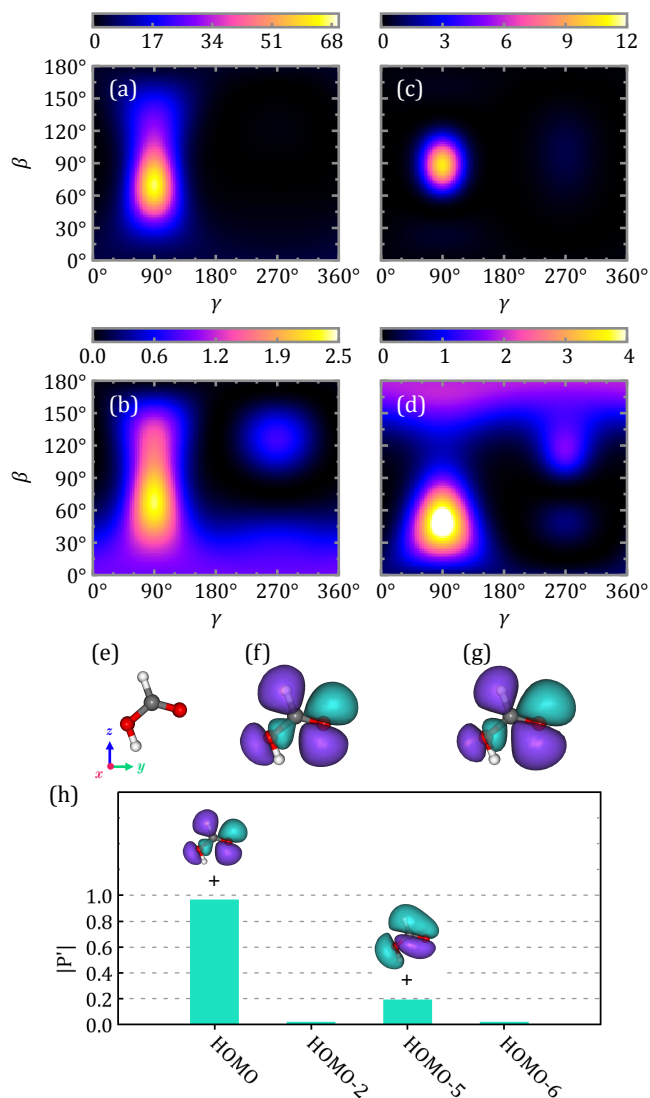


FIG. 5. Structure factors $|G_{00}|^2$ from (a) HOMO, (c) HOMO-4, and (d) HOMO-5 of HCOOH calculated using OE-WFAT. The magnitude of $|G_{00}|^2$'s in panel (c) and (d) have been divided by 100. (b) $|G_{00}|^2$ calculated by ME-WFAT. (e) Image of the HCOOH molecule as well as the z -axis which determines the $(0^\circ, 0^\circ)$ direction. (f) The HOMO used to calculate the $|G_{00}|^2$ in (a). (g) The Dyson orbital used to calculate the $|G_{00}|^2$ in (b). (h) The values of $\mathcal{P}^i(i) = (-1)^i \mathcal{P}(i)$ of several MO with the largest contribution to the Dyson orbital. The sign symbol above each bar indicates its sign. The orbital picture shown above the sign symbol is the shape of the corresponding neutral orbital.

symmetry, where the axis of the three-fold rotational symmetry coincides with the CF bond. The C–F and C–H bond lengths are 1.360 Å and 1.080 Å, respectively, with the HCF angle of 108.93°. Its HOMO is doubly degenerate and can be identified based on their reflection symmetry with respect to one of the three FCH planes. Unlike the degenerate HOMO of OCS and O₂, the two

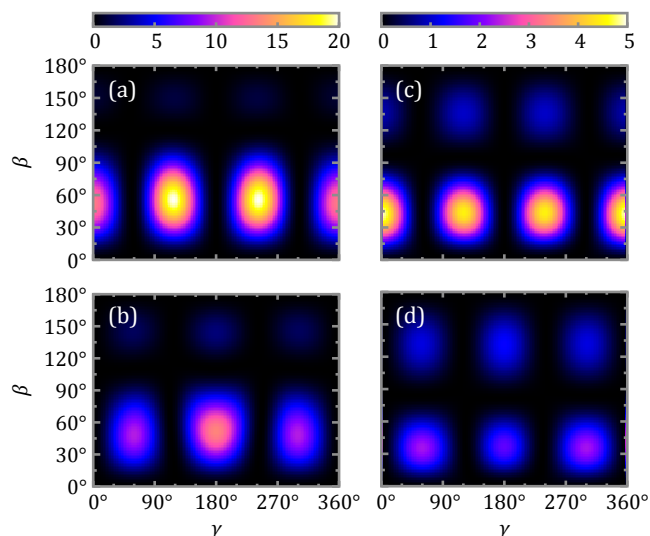


FIG. 6. (a) and (b): $|G_{00}|^2$ of CH₃F obtained by OE-WFAT using the two degenerate HOMO of the neutral molecule, respectively. (c) and (d): $|G_{00}|^2$ of CH₃F obtained by ME-WFAT using the two degenerate ground states of the cation, respectively. These degenerate states are constructed at every orientation angle so that they diagonalize one-particle (in OE-WFAT) or all-particle (in ME-WFAT) dipole matrix.

degenerate HOMO of CH₃F do not diagonalize the dipole matrix, therefore, in view of the perturbation theory, a diagonalization of the dipole matrix in the subspace of degenerate HOMO (in OE-WFAT) or in the subspace of degenerate CH₃F⁺ ground state (in ME-WFAT) must be performed at every orientation angle. The eigenvectors are then used in the WFAT integral formula—for ME-WFAT, these eigenvectors are used as $|\Psi^+\rangle$ wherever it appears. In practice, these dipole-diagonalizing states are never actually constructed at every orientation angle, which would otherwise require the expensive WFAT integrals (Eq. (41)) to be recomputed too. This is possible since structure factors are linear with respect to $|\Psi^+\rangle$. Therefore, the transformation can be applied to the structure factors of the non-diagonalizing states, avoiding the recomputation of WFAT integrals.

Fig. 6(a) and 6(b) show the $|G_{00}|^2$ structure factors obtained by OE-WFAT using the two degenerate HOMO of CH₃F that diagonalize the one-particle dipole matrix. While Fig. 6(c) and 6(d) are the ME-WFAT counterparts obtained using the two degenerate ground states of CH₃F⁺ that diagonalize the total (all-particle) dipole matrix. Both OE-WFAT and ME-WFAT structure factors in Fig. 6 exhibit the three-fold rotational symmetry of the molecule. We note in passing that the individual state's structure factors calculated without diagonalizing the dipole matrix do not exhibit the three-fold rotational symmetry but still lead to identical total structure factor as those in Fig. 6.

Apart from the intensity, the most noticeable difference between the OE-WFAT and ME-WFAT results in

Fig. 6 are the sizes and locations of the lobes, with ME-WFAT structure factors having smaller lobes than OE-WFAT and are located at a smaller β . Upon closer inspection, it can also be seen that the three lobes in the ME-WFAT results are more uniform in shape than those in OE-WFAT. We attribute this observation to the direction of the dipole moment vectors. Due to the approximate nature of the electronic structure computation, the dipole vectors of the degenerate CH_3F HOMO (as used by OE-WFAT) are numerically less parallel to the C_3 axis of the molecule than the dipole vectors of the neutral's ground state and the cation's degenerate ground states (as used by ME-WFAT).

The strong-field ionization of CH_3F has previously been studied using time-dependent configuration interaction singles with a quasi-static field in Ref. [82], where the angle-resolved ionization rate is found to have a peak around $\beta \sim 39^\circ$ for low intensity cases. In this regard, ME-WFAT agrees more closely with $\beta = 42^\circ$ (see Fig. 6(c) and 6(d)) than OE-WFAT with $\beta = 52^\circ$ (see Fig. 6(a) and 6(b)).

V. CONCLUSIONS AND OUTLOOK

In the present work, we have derived ME-WFAT using the integral representation (IR), allowing for the computation of tunnel ionization in molecules of arbitrary geometries. This development extends the previous version of ME-WFAT formulated using the tail representation (TR) [47], where the need for an accurate asymptotic part of the wave functions makes its applicability to systems other than atoms, diatomics, or simple linear molecules difficult. We have presented some test cases covering atoms, as well as linear, planar, and C_{3v} -symmetry-possessing molecules to demonstrate its capabilities. The integral formulation outlined in the present work also underlies our recent work on the application of IR ME-WFAT to the DFT wave function [53].

We find that the asymptotic coefficients of He, Li, Be, Na, and Mg calculated by IR ME-WFAT generally agree with TR ME-WFAT values with the largest relative error of about 6% for the atoms calculated in this work (see Table II). The difference can be attributed to the level of theory with which the initial and final wave functions are calculated, which is only at the HF level in this work. This suggests that the equivalence between TR and IR ME-WFAT should generally improve as more accurate wave functions are used.

The main factors that can make the angular dependence of the ionization yield calculated by OE-WFAT and ME-WFAT noticeably differ are (i) the ionizing orbital (the Dyson orbital in ME-WFAT and a MO in OE-WFAT), (ii) the dipole moments, or a combination of both. The structure factors calculated by OE-WFAT and ME-WFAT are in very good agreement if the Dyson orbital is close to the HOMO and the HOMO dipole moment is similar to the difference between total initial and

final state's dipole moment. An example of such molecule is O_2 . When the difference in (ii) is more prominent, new features will appear in ME-WFAT structure factors not seen in OE-WFAT (N_2 , HCOOH , and CH_3F are examples in this category), which include producing a totally different shape for the structure factor. From our analysis on N_2 (Section IV D), we see that ME-WFAT has the property such that it tends to select the most appropriate ionizing orbital having the right symmetry as verified by experiments.

One obvious direction for improvement in the formulation we have presented is to include the first order correction to $f_{\nu\sigma}^{n'n}$ to simulate the effect of the distortion of the wave functions on the ionization probability – this has been done in the TR ME-WFAT [62]. The inclusion of this induced effect will modify the effective dipole moment of the molecule, which will in turn affect the net force that drives the ionized electron. Another prospect is the use of multiconfiguration wave functions, which has been found to pose a problem for TR ME-WFAT [49]. In particular, IR ME-WFAT can be used to accurately calculate ionization from molecules dominated by multireference configurations, such as those containing transition metals, provided accurate multireference wave functions are provided. Apart from the possibility of studying correlation effects in tunnel ionization, ME-WFAT with multiconfiguration wave functions also enables one to ionize from an excited initial state. This is expected to become increasingly important as field strength increases as more and more excited levels of the neutral will get populated.

ACKNOWLEDGMENTS

We thank Oleg Tolstikhin for the enlightening discussion about the origin-invariance property of the WFAT. The author is also grateful to Takeshi Sato for his suggestions regarding the degenerate Hartree-Fock solutions of CH_3F^+ . This work was supported by the U.S. Department of Energy, Office of Science, Office of Basic Energy Sciences, under Award No. DE-SC0012462. Portions of this research were conducted with high performance computational resources provided by Louisiana State University and the Louisiana Optical Network Infrastructure.

Appendix A: INTEGRAL FORMULAE FOR SINGLE-DETERMINANT WAVE FUNCTIONS

To derive integral formulae for single determinant wave functions, we will first write down the single-determinant wave functions of Eq. (45) in terms of their respective Laplace expansion containing Slater determinants of $N -$

2 electrons,

$$\begin{aligned} \Psi(Q_N) &= \frac{1}{\sqrt{N(N-1)}} \sum_{\sigma_j} \sum_{j=1}^{N_{\sigma_j}} (-1)^{N+\bar{j}} \psi_j^{\sigma_j}(q) \\ &\times \sum_{\sigma_k} \sum_{k \in \mathcal{K}_j} (-1)^{1+\bar{k}_j} \psi_k^{\sigma_k}(q_1) \\ &\times \Psi[\psi_j^{\sigma_j}, \psi_k^{\sigma_k}](Q_{N-2}) \end{aligned} \quad (\text{A1})$$

$$\begin{aligned} \Psi^+(Q_{N-1}) &= \frac{1}{\sqrt{N-1}} \sum_{\sigma_{k'}} \sum_{k'=1}^{N'_{\sigma_{k'}}} (-1)^{1+\bar{k}'} v_{k'}^{\sigma_{k'}}(q_1) \\ &\times \Psi^+[v_{k'}^{\sigma_{k'}}](Q_{N-2}), \end{aligned} \quad (\text{A2})$$

where

$$\bar{j} = \delta_{\sigma\beta} N_\alpha + j, \quad (\text{A3a})$$

$$\mathcal{K}_j \equiv \begin{cases} \{k | k \in \mathbb{Z}, 1 \leq k \leq N_{\sigma_k}\} & , \sigma_k \neq \sigma_j, \\ \{k | k \in \mathbb{Z}, 1 \leq k \leq N_{\sigma_k}, k \neq j\} & , \sigma_k = \sigma_j, \end{cases} \quad (\text{A3b})$$

$$\bar{k}_j = \begin{cases} \bar{k} & , \bar{k} < \bar{j} \\ \bar{k} - 1 & , \bar{k} > \bar{j} \end{cases}, \quad (\text{A3c})$$

$$\bar{k} = \delta_{\sigma\beta} N_\alpha + k, \quad (\text{A3d})$$

$$\bar{k}' = \delta_{\sigma\beta} N'_\alpha + k', \quad (\text{A3e})$$

and $A[a, b, \dots, z]$ denotes a Slater determinant formed by removing a, b, \dots, z spin orbitals from Slater determinant A . Although it has no physical significance, the assumption introduced in the beginning of Section III F on the order of the columns of the matrix yielding the Slater

determinants is respected in Eqs. (A1) and (A2). Eqs. (A3) are subject to this spin orbital ordering assumption, that is, different ordering will give different signs of each term in the above Laplace expansions. Such a difference in the sign will, however, only affect the overall sign of the asymptotic coefficient, while the ionization rate, which is an observable, will remain unchanged.

Next, we will introduce the following definitions

$$\mathcal{P}(i) = \det \left(S_\sigma^{\Psi^+ \Psi} \left[\emptyset \middle| \psi_i^\sigma \right] \right), \quad (\text{A4a})$$

$$\mathcal{R} = \det \left(S_{p(\sigma)}^{\Psi^+ \Psi} \left[\emptyset \middle| \psi_i^\sigma \right] \right), \quad (\text{A4b})$$

$$\mathcal{Q}(k, i, k') = \det \left(S_\sigma^{\Psi^+ \Psi} \left[v_{k'}^\sigma \middle| \psi_i^\sigma, \psi_k^\sigma \right] \right) (1 - \delta_{ik}), \quad (\text{A4c})$$

$$\mathcal{S}(k, k') = \det \left(S_{p(\sigma)}^{\Psi^+ \Psi} \left[v_{k'}^{p(\sigma)} \middle| \psi_i^\sigma, \psi_k^{p(\sigma)} \right] \right). \quad (\text{A4d})$$

The notation $S_\sigma^{\Psi^+ \Psi} [a', b', \dots | a, b, \dots]$ denotes the spin- σ block of the overlap matrix formed between the orbitals occupied in $|\Psi^+\rangle$ removing spin-orbitals a', b', \dots and the orbitals occupied in $|\Psi\rangle$ removing spin-orbitals a, b, \dots . The number of orbitals removed from the two wave functions has been ensured such that the resulting modified overlap matrix is square. Note that \mathcal{R} and \mathcal{S} are independent of ψ_i^σ , hence \mathcal{R} is a scalar. We will also rewrite the 2-electron potential term in Eq. (20) as

$$\begin{aligned} V_{2e}(\mathbf{R}_N) &= \sum_{i=1}^{N-1} U_{2e}(\mathbf{r}_i, \mathbf{r}), \\ U_{2e}(\mathbf{r}_i, \mathbf{r}) &= \frac{1}{|\mathbf{r} - \mathbf{r}_i|}. \end{aligned}$$

The 2-electron contribution to the integral of Eq. (41) from the $U_{2e}(\mathbf{r}_1, \mathbf{r})$ term is

$$\begin{aligned} \langle \Psi^+; \Omega_{lm'}^\nu \chi_\sigma \left| \hat{U}_{2e}(\hat{\mathbf{r}}_1, \hat{\mathbf{r}}) \right| \Psi \rangle &= \frac{1}{\sqrt{N(N-1)}} \sum_{\sigma_k} \sum_{k'=1}^{N'_{\sigma_k}} \sum_{j=1}^{N_\sigma} \sum_{k \in \mathcal{K}_j} (-1)^{N+\bar{k}'+\bar{j}+\bar{k}_j} \langle \Psi^+ [v_{k'}^{\sigma_k}] | \Psi [\psi_j^\sigma, \psi_k^{\sigma_k}] \rangle \\ &\times \int d^3\mathbf{r} (\Omega_{lm'}^\nu(\mathbf{r}))^* \langle v_{k'}^{\sigma_k} | \hat{U}_{2e}(\hat{\mathbf{r}}_1, \mathbf{r}) | \psi_k^{\sigma_k} \rangle \psi_j^\sigma(\mathbf{r}) \\ &= \frac{\delta_{M'_s+m_\sigma, M_s}}{\sqrt{N(N-1)}} (-1)^N \left\{ \mathcal{R} \sum_{k'=1}^{N'_\sigma} \sum_{j=1}^{N_\sigma} \sum_{k \neq j}^{N_\sigma} (-1)^{\bar{j}+\bar{k}'+\bar{k}_j} \mathcal{Q}(k, j, k') \langle \Omega_{lm'}^\nu | \hat{V}_{k'k}^\sigma | \psi_j^\sigma \rangle \right. \\ &\quad \left. + \langle \Omega_{lm'}^\nu | \left(\sum_{k'=1}^{N_{p(\sigma)}} \sum_{k=1}^{N_{p(\sigma)}} (-1)^{\bar{k}'+\bar{k}_j} \mathcal{S}(k', k) \hat{V}_{k'k}^{p(\sigma)} \right) \left(\sum_{j=1}^{N_\sigma} (-1)^{\bar{j}} \mathcal{P}(j) | \psi_j^\sigma \rangle \right) \right\} \\ &= \frac{\delta_{M'_s+m_\sigma, M_s}}{\sqrt{N(N-1)}} (-1)^{N+\delta_{\sigma\beta} N_\alpha} \left\{ \mathcal{R} \sum_{k'=1}^{N_\sigma-1} \sum_{j=2}^{N_\sigma} \sum_{k=1}^{j-1} (-1)^{j+k+k'} \mathcal{Q}(k, j, k') \right. \\ &\quad \left. \times \left(\langle \Omega_{lm'}^\nu | \hat{V}_{k'k}^\sigma | \psi_j^\sigma \rangle - \langle \Omega_{lm'}^\nu | \hat{V}_{k'j}^\sigma | \psi_k^\sigma \rangle \right) + \langle \Omega_{lm'}^\nu | \hat{\gamma}^\sigma | \tilde{\psi}^\sigma \rangle \right\}. \end{aligned} \quad (\text{A5})$$

where

$$\tilde{\psi}^\sigma(\mathbf{r}) = \sum_{i=1}^{N_\sigma} (-1)^i \mathcal{P}(i) \psi_i^\sigma(\mathbf{r}), \quad (\text{A6})$$

$$\mathcal{V}^\sigma(\mathbf{r}) = \sum_{k'=1}^{N_{p(\sigma)}} \sum_{k=1}^{N_{p(\sigma)}} (-1)^{k'+k} \mathcal{S}(k', k) V_{k'k}^{p(\sigma)}(\mathbf{r}), \quad (\text{A7})$$

$$V_{k'i}^\sigma(\mathbf{r}) = \int d^3\mathbf{r}' (v_{k'}^\sigma(\mathbf{r}'))^* \frac{1}{|\mathbf{r}-\mathbf{r}'|} \psi_i^\sigma(\mathbf{r}'). \quad (\text{A8})$$

In the second equality in Eq. (A5), we use the relation that the overlap between two Slater determinants is equal to the determinant of the overlap matrix formed by the orbitals making up each determinant,

$$\begin{aligned} & \langle \Psi^+ [v_{k'}^{\sigma_k}] | \Psi [\psi_j^\sigma, \psi_k^{\sigma_k}] \rangle \\ &= \det \left(S_{p(\sigma_k)}^{\Psi^+ \Psi} [\emptyset | \psi_j^\sigma] \right) \det \left(S_{\sigma_k}^{\Psi^+ \Psi} [v_{k'}^{\sigma_k} | \psi_j^\sigma, \psi_k^{\sigma_k}] \right) \\ &= \begin{cases} \mathcal{R} \mathcal{Q}(k, j, k') & , \sigma_k = \sigma \\ \mathcal{P}(j) \mathcal{S}(k', k) & , \sigma_k \neq \sigma \end{cases}, \end{aligned}$$

while in the last equality of the same equation, we use the symmetry property of \mathcal{Q} , which is $\mathcal{Q}(k, j, k') = \mathcal{Q}(j, k, k')$. In this step, we have also expanded \bar{j} , \bar{k}' , and \bar{k} based on whether $\sigma_k = \sigma$ or $\sigma_k = p(\sigma)$. Because the last expression of Eq. (A5) is independent of electron index, the total 2-electron contribution is then

$$\begin{aligned} \langle \Psi^+; \Omega_{lm'}^\nu \chi_\sigma | \hat{V}_{2e} | \Psi \rangle &= (N-1) \\ &\times \langle \Psi^+; \Omega_{lm'}^\nu \chi_\sigma | \hat{U}_{2e}(\hat{\mathbf{r}}_1, \hat{\mathbf{r}}) | \Psi \rangle. \end{aligned}$$

The 1-electron contribution is much more straightforward

to derive,

$$\begin{aligned} & \langle \Psi^+; \Omega_{lm'}^\nu \chi_\sigma | \hat{V}_{1e} | \Psi \rangle \\ &= \frac{1}{\sqrt{N}} \sum_{j=1}^{N_\sigma} (-1)^{N+j} \langle \Psi^+ | \Psi [\psi_j^\sigma] \rangle \langle \Omega_{lm'}^\nu | \hat{V}_{1e} | \psi_j^\sigma \rangle \\ &= \frac{(-1)^{N+\delta_{\sigma\beta} N_\alpha}}{\sqrt{N}} \sum_{j=1}^{N_\sigma} (-1)^j \mathcal{R} \mathcal{P}(j) \langle \Omega_{lm'}^\nu | \hat{V}_{1e} | \psi_j^\sigma \rangle \\ &= \delta_{M'_s+m_\sigma, M_s} \langle \Omega_{lm'}^\nu | \hat{V}_{1e} | \psi_D^\sigma \rangle, \quad (\text{A9}) \end{aligned}$$

where

$$\psi_D^\sigma(\mathbf{r}) = \frac{(-1)^{N+\delta_{\sigma\beta} N_\alpha}}{\sqrt{N}} \mathcal{R} \tilde{\psi}^\sigma(\mathbf{r}). \quad (\text{A10})$$

ψ_D^σ is the Dyson orbital corresponding to the removal of an electron from the spin- σ channel of the initial HF wave function. The appearance of $\delta_{M'_s+m_\sigma, M_s}$ in Eq. (A5) and (A9) accounts for the fact that Slater determinants are eigenstates of the z projection of the total spin angular momentum operator, and that \hat{V}_{2e} and \hat{V}_{1e} do not depend on any spin operators.

We note that the $\mathcal{P}(i)$'s encode the contribution of orbitals to the ionization rate through the Dyson orbital (see Eqs. (A10) and (A6)). On the other hand, orbital energy is also often used as a measure of contribution of that orbital to the rate. Nevertheless, orbital energy and $\mathcal{P}(i)$ are independent of each other. But they independently determine the overall contribution of an orbital to the rate—the energies affect the asymptotic behavior through the exponential tail, while the $\mathcal{P}(i)$'s determine the shape of the ionizing orbital, that is, the Dyson orbital.

Appendix B: OBTAINING OE-WFAT INTEGRAL FORMULA FROM ME-WFAT

Using Eq. (49) in Eq. (47), we may derive for the 2-electron term

$$\begin{aligned}
\langle \Psi^+; \Omega_{lm'}^\nu \chi_\sigma | \hat{V}_{2e} | \Psi \rangle &= \frac{(-1)^{N+\delta_{\sigma 2} N_1+i'}}{\sqrt{N}} \langle \Omega_{lm'}^\nu | \left\{ \sum_{k'=1}^{N_\sigma-1} \sum_{k=1}^{i'-1} (-1)^{k+k'} \delta_{k'k} \left(\hat{V}_{k'k}^\sigma |\psi_{i'}^\sigma\rangle - \hat{V}_{k'i'}^\sigma |\psi_k^\sigma\rangle \right) \right. \\
&\quad \left. + \sum_{k'=1}^{N_\sigma-1} \sum_{j=i'+1}^{N_\sigma} (-1)^{j+k'} \delta_{k',j-1} \left(\hat{V}_{k'i'}^\sigma |\psi_j^\sigma\rangle - \hat{V}_{k'j}^\sigma |\psi_{i'}^\sigma\rangle \right) + \sum_{k=1}^{N_p(\sigma)} \hat{V}_{kk}^{p(\sigma)} |\psi_{i'}^\sigma\rangle \right\} \\
&= \frac{(-1)^{N+\delta_{\sigma 2} N_1+i'}}{\sqrt{N}} \langle \Omega_{lm'}^\nu | \left\{ \sum_{k \neq i'}^{N_\sigma} \left(\hat{V}_{kk}^\sigma |\psi_{i'}^\sigma\rangle - \hat{V}_{ki'}^\sigma |\psi_k^\sigma\rangle \right) + \sum_{k=1}^{N_p(\sigma)} \hat{V}_{kk}^{p(\sigma)} |\psi_{i'}^\sigma\rangle \right\} \\
&= \frac{(-1)^{N+\delta_{\sigma 2} N_1+i'}}{\sqrt{N}} \langle \Omega_{lm'}^\nu | \left(\sum_{\sigma_k} \sum_{k=1}^{N_{\sigma_k}} \hat{V}_{kk}^{\sigma_k} |\psi_{i'}^\sigma\rangle - \sum_{k=1}^{N_\sigma} \hat{V}_{ki'}^\sigma |\psi_k^\sigma\rangle \right). \tag{B1}
\end{aligned}$$

In Eq. (B1), one may identify the first term in the parentheses to be the classical repulsion term and the second term to be the HF exchange term. While using Eq. (49)

in Eq. (48) gives the 1-electron term,

$$\begin{aligned}
\langle \Psi^+; \Omega_{lm'}^\nu \chi_\sigma | \hat{V}_{1e} | \Psi \rangle &= \frac{(-1)^{N+\delta_{\sigma 2} N_1+i'}}{\sqrt{N}} \\
&\quad \times \langle \Omega_{lm'}^\nu | \hat{V}_{1e} | \psi_{i'}^\sigma \rangle. \tag{B2}
\end{aligned}$$

Eq. (B1) and (B2), up to a common constant prefactor, are identical to the integral formula of OE-WFAT in the IR using the occupied orbital $|\psi_{i'}^\sigma\rangle$ obtained through HF method (compare with eqs. (32)-(34) in Ref. [50]). The sign in the prefactor is immaterial, whereas the $N^{-1/2}$ factor will be canceled by the factor N in Eq. (44) upon calculating the ionization rate.

-
- [1] M. S. Misha Yu Ivanov and O. Smirnova, Anatomy of strong field ionization, *J. Mod. Opt.* **52**, 165 (2005).
 - [2] S. V. Popruzhenko, Keldysh theory of strong field ionization: history, applications, difficulties and perspectives, *J. Phys. B* **47**, 204001 (2014).
 - [3] C. I. Blaga, F. Catoire, P. Colosimo, G. G. Paulus, H. G. Muller, P. Agostini, and L. F. DiMauro, Strong-field photoionization revisited, *Nat. Phys.* **5**, 335–338 (2009).
 - [4] J. Wiese, J. Onvlee, S. Trippel, and J. Küpper, Strong-field ionization of complex molecules, *Phys. Rev. Res.* **3**, 013089 (2021).
 - [5] A. McPherson, G. Gibson, H. Jara, U. Johann, T. S. Luk, I. A. McIntyre, K. Boyer, and C. K. Rhodes, Studies of multiphoton production of vacuum-ultraviolet radiation in the rare gases, *J. Opt. Soc. Am. B* **4**, 595 (1987).
 - [6] J. L. Krause, K. J. Schafer, and K. C. Kulander, Calculation of photoemission from atoms subject to intense laser fields, *Phys. Rev. A* **45**, 4998 (1992).
 - [7] M. V. Ammosov, N. B. Delone, and V. P. Krainov, Tunnel Ionization Of Complex Atoms And Atomic Ions In Electromagnetic Field, in *High Intensity Laser Processes*, Vol. 0664, edited by J. A. Alcock, International Society for Optics and Photonics (SPIE, 1986) pp. 138 – 141.
 - [8] X. M. Tong, Z. X. Zhao, and C. D. Lin, Theory of molecular tunneling ionization, *Phys. Rev. A* **66**, 033402 (2002).
 - [9] T. K. Kjeldsen, C. Z. Bisgaard, L. B. Madsen, and H. Stapelfeldt, Influence of molecular symmetry on strong-field ionization: Studies on ethylene, benzene, fluorobenzene, and chlorofluorobenzene, *Phys. Rev. A* **71**, 013418 (2005).
 - [10] L. V. Keldysh, Ionization in the field of a strong electromagnetic wave, in *Selected Papers of Leonid V Keldysh*, pp. 56–63.
 - [11] F. H. M. Faisal, Multiple absorption of laser photons by atoms, *J. Phys. B* **6**, L89 (1973).
 - [12] H. R. Reiss, Effect of an intense electromagnetic field on a weakly bound system, *Phys. Rev. A* **22**, 1786 (1980).
 - [13] O. I. Tolstikhin, T. Morishita, and L. B. Madsen, Theory of tunneling ionization of molecules: Weak-field asymptotics including dipole effects, *Phys. Rev. A* **84**, 053423 (2011).
 - [14] L. B. Madsen, O. I. Tolstikhin, and T. Morishita, Application of the weak-field asymptotic theory to the analysis of tunneling ionization of linear molecules, *Phys. Rev. A* **85**, 053404 (2012).
 - [15] V. H. Trinh, O. I. Tolstikhin, L. B. Madsen, and T. Morishita, First-order correction terms in the weak-field asymptotic theory of tunneling ionization, *Phys. Rev. A* **87**, 043426 (2013).
 - [16] L. B. Madsen, F. Jensen, O. I. Tolstikhin, and T. Mor-

- ishita, Structure factors for tunneling ionization rates of molecules, *Phys. Rev. A* **87**, 013406 (2013).
- [17] R. Saito, O. I. Tolstikhin, L. B. Madsen, and T. Morishita, Structure factors for tunneling ionization rates of diatomic molecules, *Atom. Data Nucl. Data* **103-104**, 4 (2015).
- [18] L. Greenman, P. J. Ho, S. Pabst, E. Kamarchik, D. A. Mazziotti, and R. Santra, Implementation of the time-dependent configuration-interaction singles method for atomic strong-field processes, *Phys. Rev. A* **82**, 023406 (2010).
- [19] J. Zanghellini, M. Kitzler, C. Fabian, T. Brabec, and A. Scrinzi, An mctdhf approach to multielectron dynamics in laser fields, *Laser Phys.* **13**, 1064 (2003).
- [20] T. Kato and H. Kono, Time-dependent multiconfiguration theory for electronic dynamics of molecules in an intense laser field, *Chem. Phys. Lett.* **392**, 533 (2004).
- [21] T. Sato and K. L. Ishikawa, Time-dependent complete-active-space self-consistent-field method for multielectron dynamics in intense laser fields, *Phys. Rev. A* **88**, 023402 (2013).
- [22] H. Miyagi and L. B. Madsen, Time-dependent restricted-active-space self-consistent-field theory for laser-driven many-electron dynamics, *Phys. Rev. A* **87**, 062511 (2013).
- [23] T. Sato and K. L. Ishikawa, Time-dependent multi-configuration self-consistent-field method based on the occupation-restricted multiple-active-space model for multielectron dynamics in intense laser fields, *Phys. Rev. A* **91**, 023417 (2015).
- [24] R. Kosloff and D. Kosloff, Absorbing boundaries for wave propagation problems, *J. Comput. Phys.* **63**, 363 (1986).
- [25] D. Neuhaser and M. Baer, The time-dependent Schrödinger equation: Application of absorbing boundary conditions, *J. Chem. Phys.* **90**, 4351 (1989).
- [26] U. V. Riss and H. Meyer, Investigation on the reflection and transmission properties of complex absorbing potentials, *J. Chem. Phys.* **105**, 1409 (1996).
- [27] P. Krause, J. A. Sonk, and H. B. Schlegel, Strong field ionization rates simulated with time-dependent configuration interaction and an absorbing potential, *J. Chem. Phys.* **140**, 174113 (2014).
- [28] P. Krause and H. B. Schlegel, Strong-field ionization rates of linear polyenes simulated with time-dependent configuration interaction with an absorbing potential, *J. Chem. Phys.* **141**, 174104 (2014).
- [29] P. Krause and H. B. Schlegel, Angle-dependent ionization of small molecules by time-dependent configuration interaction and an absorbing potential, *J. Phys. Chem. Lett.* **6**, 2140 (2015).
- [30] A. S. Durden and H. B. Schlegel, Reducing the Cost of TD-CI Simulations of Strong Field Ionization, *J. Phys. Chem. A* **128**, 7440 (2024).
- [31] F. He, C. Ruiz, and A. Becker, Absorbing boundaries in numerical solutions of the time-dependent Schrödinger equation on a grid using exterior complex scaling, *Phys. Rev. A* **75**, 053407 (2007).
- [32] L. Tao, W. Vanroose, B. Reys, T. N. Rescigno, and C. W. McCurdy, Long-time solution of the time-dependent Schrödinger equation for an atom in an electromagnetic field using complex coordinate contours, *Phys. Rev. A* **80**, 063419 (2009).
- [33] A. Scrinzi, Infinite-range exterior complex scaling as a perfect absorber in time-dependent problems, *Phys. Rev. A* **81**, 053845 (2010).
- [34] Y. Orimo, T. Sato, A. Scrinzi, and K. L. Ishikawa, Implementation of the infinite-range exterior complex scaling to the time-dependent complete-active-space self-consistent-field method, *Phys. Rev. A* **97**, 023423 (2018).
- [35] L. B. Madsen, L. A. A. Nikolopoulos, T. K. Kjeldsen, and J. Fernández, Extracting continuum information from $\Psi(t)$ in time-dependent wave-packet calculations, *Phys. Rev. A* **76**, 063407 (2007).
- [36] M. Abu-samha and L. B. Madsen, Alignment dependence of photoelectron momentum distributions of atomic and molecular targets probed by few-cycle circularly polarized laser pulses, *Phys. Rev. A* **94**, 023414 (2016).
- [37] M. Abu-samha and L. B. Madsen, Interplay between pulse parameters and alignment of H_2^+ in strong laser fields, *Journal of Physics: Conference Series* **869**, 012009 (2017).
- [38] M. Abu-samha and L. B. Madsen, Multielectron effects in strong-field ionization of the oriented OCS molecule, *Phys. Rev. A* **102**, 063111 (2020).
- [39] M. Abu-samha and L. B. Madsen, Strong-field ionization and AC-Stark shifted Rydberg states in OCS, *J. Phys. B* **56**, 105401 (2023).
- [40] K. Lopata and N. Govind, Modeling fast electron dynamics with real-time time-dependent density functional theory: Application to small molecules and chromophores, *J. Chem. Theory Comput.* **7**, 1344 (2011).
- [41] A. Sissay, P. Abanador, F. Mauger, M. Gaarde, K. J. Schafer, and K. Lopata, Angle-dependent strong-field molecular ionization rates with tuned range-separated time-dependent density functional theory, *J. Chem. Phys.* **145**, 094105 (2016).
- [42] P. Kraus, O. I. Tolstikhin, D. Baykusheva, A. Rupenyan, J. Schneider, C. Z. Bisgaard, T. Morishita, F. Jensen, L. B. Madsen, and H. J. Wörner, Observation of laser-induced electronic structure in oriented polyatomic molecules, *Nat. Commun.* **6**, 7039 (2015).
- [43] P. M. Kraus, B. Mignolet, D. Baykusheva, A. Rupenyan, L. Horný, E. F. Penka, G. Grassi, O. I. Tolstikhin, J. Schneider, F. Jensen, L. B. Madsen, A. D. Bandrauk, F. Remacle, and H. J. Wörner, Measurement and laser control of attosecond charge migration in ionized iodoacetylene, *Science* **350**, 790 (2015).
- [44] T. Endo, H. Fujise, H. Hasegawa, A. Matsuda, M. Fushitani, O. I. Tolstikhin, T. Morishita, and A. Hishikawa, Angle dependence of dissociative tunneling ionization of NO in asymmetric two-color intense laser fields, *Phys. Rev. A* **100**, 053422 (2019).
- [45] A. Tehlar, J. T. Casanova, A. Dnestryan, F. Jensen, L. B. Madsen, O. I. Tolstikhin, and H. J. Wörner, High-harmonic spectroscopy of impulsively aligned 1,3-cyclohexadiene: Signatures of attosecond charge migration, *Struct. Dyn.* **11**, 014304 (2024).
- [46] A. I. Dnestryan and O. I. Tolstikhin, Integral-equation approach to the weak-field asymptotic theory of tunneling ionization, *Phys. Rev. A* **93**, 033412 (2016).
- [47] O. I. Tolstikhin, L. B. Madsen, and T. Morishita, Weak-field asymptotic theory of tunneling ionization in many-electron atomic and molecular systems, *Phys. Rev. A* **89**, 013421 (2014).
- [48] L. Yue, S. Bauch, and L. B. Madsen, Electron correlation in tunneling ionization of diatomic molecules: An application of the many-electron weak-field asymptotic theory with a generalized-active-space partition scheme,

- Phys. Rev. A* **96**, 043408 (2017).
- [49] I. Y. Tolstikhina, T. Morishita, and O. I. Tolstikhin, Application of the many-electron weak-field asymptotic theory of tunneling ionization to atoms, *Phys. Rev. A* **90**, 053413 (2014).
- [50] L. B. Madsen, F. Jensen, A. I. Dnestryan, and O. I. Tolstikhin, Structure factors for tunneling ionization rates of molecules: General hartree-fock-based integral representation, *Phys. Rev. A* **96**, 013423 (2017).
- [51] A. I. Dnestryan, O. I. Tolstikhin, L. B. Madsen, and F. Jensen, Structure factors for tunneling ionization rates of molecules: General grid-based methodology and convergence studies, *J. Chem. Phys.* **149**, 164107 (2018).
- [52] A. I. Dnestryan, O. I. Tolstikhin, F. Jensen, and L. B. Madsen, Torsional effects in strong-field ionization of molecules, *Phys. Rev. Research* **1**, 023018 (2019).
- [53] I. S. Wahyutama, D. D. Jayasinghe, F. Mauger, K. Lopata, M. B. Gaarde, and K. J. Schafer, All-electron, density-functional-based method for angle-resolved tunneling ionization in the adiabatic regime, *Phys. Rev. A* **106**, 052211 (2022).
- [54] M. Valiev, E. Bylaska, N. Govind, K. Kowalski, T. Straatsma, H. Van Dam, D. Wang, J. Nieplocha, E. Apra, T. Windus, and W. de Jong, Nwchem: A comprehensive and scalable open-source solution for large scale molecular simulations, *Comput. Phys. Commun.* **181**, 1477 (2010).
- [55] E. Aprà, E. J. Bylaska, W. A. de Jong, N. Govind, K. Kowalski, T. P. Straatsma, M. Valiev, H. J. J. van Dam, Y. Alexeev, J. Anchell, V. Anisimov, F. W. Aquino, R. Atta-Fynn, J. Autschbach, N. P. Bauman, J. C. Becca, D. E. Bernholdt, K. Bhaskaran-Nair, S. Bogatko, P. Borowski, J. Boschen, J. Brabec, A. Bruner, E. Cauët, Y. Chen, G. N. Chuev, C. J. Cramer, J. Daily, M. J. O. Deegan, J. Dunning, T. H., M. Dupuis, K. G. Dyall, G. I. Fann, S. A. Fischer, A. Fonari, H. Früchtl, L. Gagliardi, J. Garza, N. Gawande, S. Ghosh, K. Glaesemann, A. W. Götz, J. Hammond, V. Helms, E. D. Hermes, K. Hirao, S. Hirata, M. Jacquelin, L. Jensen, B. G. Johnson, H. Jónsson, R. A. Kendall, M. Klemm, R. Kobayashi, V. Konkov, S. Krishnamoorthy, M. Krishnan, Z. Lin, R. D. Lins, R. J. Littlefield, A. J. Logsdail, K. Lopata, W. Ma, A. V. Marenich, J. Martin del Campo, D. Mejia-Rodriguez, J. E. Moore, J. M. Mullin, T. Nakajima, D. R. Nascimento, J. A. Nichols, P. J. Nichols, J. Nieplocha, A. Otero-de-la Roza, B. Palmer, A. Panyala, T. Pirojsirikul, B. Peng, R. Peverati, J. Pittner, L. Pollack, R. M. Richard, P. Sadayappan, G. C. Schatz, W. A. Shelton, D. W. Silverstein, D. M. A. Smith, T. A. Soares, D. Song, M. Swart, H. L. Taylor, G. S. Thomas, V. Tipparaju, D. G. Truhlar, K. Tsemekhman, T. Van Voorhis, A. Vázquez-Mayagoitia, P. Verma, O. Villa, A. Vishnu, K. D. Vogiatzis, D. Wang, J. H. Weare, M. J. Williamson, T. L. Windus, K. Woliński, A. T. Wong, Q. Wu, C. Yang, Q. Yu, M. Zacharias, Z. Zhang, Y. Zhao, and R. J. Harrison, NWChem: Past, present, and future, *J. Chem. Phys.* **152**, 184102 (2020).
- [56] S. Song, M. Zhu, H. Ni, and J. Wu, PyStructureFactor: A Python code for the molecular structure factor in tunneling ionization rates, *Comput. Phys. Commun.* **292**, 108882 (2023).
- [57] B. Zhang and Z. Zhao, SLIMP: Strong laser interaction model package for atoms and molecules, *Comput. Phys. Commun.* **192**, 330 (2015).
- [58] Z. Ren, B. Zhang, Y. Yang, Y. Zhu, G. Bai, J. Liu, J. Zhao, and Z. Zhao, SLIMP 2.0: A new version of strong laser interaction model package for atoms and molecules, now with molecular orbital tomography based on high-order harmonic spectra, *Comput. Phys. Commun.* **301**, 109213 (2024).
- [59] I. S. Wahyutama, T. Sato, and K. L. Ishikawa, Time-dependent multiconfiguration self-consistent-field study on resonantly enhanced high-order harmonic generation from transition-metal elements, *Phys. Rev. A* **99**, 063420 (2019).
- [60] V. V. Kim, G. S. Boltaev, M. Iqbal, N. A. Abbasi, H. Al-Harmi, I. S. Wahyutama, T. Sato, K. L. Ishikawa, R. A. Ganeev, and A. S. Alnaser, Resonance enhancement of harmonics in the vicinity of 32 nm spectral range during propagation of femtosecond pulses through the molybdenum plasma, *J. Phys. B* **53**, 195401 (2020).
- [61] J. Kobus, L. Laaksonen, and D. Sundholm, A numerical hartree-fock program for diatomic molecules, *Comput. Phys. Commun.* **98**, 346 (1996).
- [62] V. H. Trinh, O. I. Tolstikhin, and T. Morishita, First-order correction terms in the weak-field asymptotic theory of tunneling ionization in many-electron systems, *J. Phys. B* **49**, 195603 (2016).
- [63] G. B. Arfken and H. J. Weber, *Mathematical Methods for Physicists* (Elsevier Science, 2013).
- [64] D. Dimitrovski, C. P. J. Martiny, and L. B. Madsen, Strong-field ionization of polar molecules: Stark-shift-corrected strong-field approximation, *Phys. Rev. A* **82**, 053404 (2010).
- [65] H. Li, D. Ray, S. De, I. Znakovskaya, W. Cao, G. Laurent, Z. Wang, M. F. Kling, A. T. Le, and C. L. Cocke, Orientation dependence of the ionization of CO and NO in an intense femtosecond two-color laser field, *Phys. Rev. A* **84**, 043429 (2011).
- [66] V.-H. Hoang, S.-F. Zhao, V.-H. Le, and A.-T. Le, Influence of permanent dipole and dynamic core-electron polarization on tunneling ionization of polar molecules, *Phys. Rev. A* **95**, 023407 (2017).
- [67] D. A. Varshalovich, A. N. Moskalev, and V. K. Khersonskii, *Quantum Theory of Angular Momentum* (World Scientific, 1988).
- [68] L. J. Slater, in *Handbook of Mathematical Functions with Formulas, Graphs, and Mathematical Tables*, edited by M. Abramowitz and I. A. Stegun (U.S. Dept. of Commerce, New York, 1972) Chap. 13.
- [69] A. D. Becke, A multicenter numerical integration scheme for polyatomic molecules, *J. Chem. Phys.* **88**, 2547 (1988).
- [70] D. Pavičić, K. F. Lee, D. M. Rayner, P. B. Corkum, and D. M. Villeneuve, Direct Measurement of the Angular Dependence of Ionization for N₂, O₂, and CO₂ in Intense Laser Fields, *Phys. Rev. Lett.* **98**, 243001 (2007).
- [71] M. Abu-samha and L. B. Madsen, Multielectron effect in the strong-field ionization of aligned nonpolar molecules, *Phys. Rev. A* **106**, 013117 (2022).
- [72] R. Johansen, K. G. Bay, L. Christensen, J. Thøgersen, D. Dimitrovski, L. B. Madsen, and H. Stapelfeldt, Alignment-dependent strong-field ionization yields of carbonyl sulfide molecules induced by mid-infrared laser pulses, *J. Phys. B* **49**, 205601 (2016).
- [73] P. Sándor, A. Sissay, F. m. c. Mauger, P. M. Abanador, T. T. Gorman, T. D. Scarborough, M. B. Gaarde, K. Lopata, K. J. Schafer, and R. R. Jones, Angle de-

- pendence of strong-field single and double ionization of carbonyl sulfide, *Phys. Rev. A* **98**, 043425 (2018).
- [74] J. L. Hansen, L. Holmegaard, J. H. Nielsen, H. Stapelfeldt, D. Dimitrovski, and L. B. Madsen, Orientation-dependent ionization yields from strong-field ionization of fixed-in-space linear and asymmetric top molecules, *J. Phys. B* **45**, 015101 (2011).
- [75] M. Abu-samha and L. B. Madsen, Effect of multielectron polarization in the strong-field ionization of the oriented co molecule, *Phys. Rev. A* **101**, 013433 (2020).
- [76] J. Wu, L. P. H. Schmidt, M. Kunitski, M. Meckel, S. Voss, H. Sann, H. Kim, T. Jahnke, A. Czasch, and R. Dörner, Multiorbital tunneling ionization of the co molecule, *Phys. Rev. Lett.* **108**, 183001 (2012).
- [77] B. Zhang, J. Yuan, and Z. Zhao, Dynamic core polarization in strong-field ionization of co molecules, *Phys. Rev. Lett.* **111**, 163001 (2013).
- [78] P. E. Cade, K. D. Sales, and A. C. Wahl, Electronic Structure of Diatomic Molecules. III. A. Hartree—Fock Wavefunctions and Energy Quantities for N_2 ($X^1\Sigma_g^+$) and N_2^+ ($X^2\Sigma_g^+$, $A^2\Pi_u$, $B^2\Sigma_u^+$) Molecular Ions, *J. Chem. Phys.* **44**, 1973 (1966).
- [79] A. Szabo and N. Ostlund, *Modern Quantum Chemistry: Introduction to Advanced Electronic Structure Theory*, Dover Books on Chemistry (Dover Publications, 1996).
- [80] M. Díaz-Tinoco, H. H. Corzo, F. Pawłowski, and J. V. Ortiz, Do Dyson Orbitals resemble canonical Hartree–Fock orbitals?, *Mol. Phys.* **117**, 2275 (2019).
- [81] For this analysis, only the angular dependence of OE-WFAT-calculated structure factors from HOMO-4 and HOMO-5 are relevant. The magnitude, however, is irrelevant because it is determined mainly by orbital energies, which are not present in the formulation of ME-WFAT.
- [82] P. Hoerner and H. B. Schlegel, Angular Dependence of Strong Field Ionization of CH_3X ($X = F, Cl, Br, \text{ or } I$) Using Time-Dependent Configuration Interaction with an Absorbing Potential, *J. Phys. Chem. A* **121**, 5940 (2017).